View metadata, citation and similar papers at core.ac.uk

brought to you by CORE

provided by NASA Technical Reports Server

NASA Technical Memorandum [illegible]290

1178

P-38

Combined Compressive and Shear Buckling Analysis of Hypersonic Aircraft Structural Sandwich Panels

William L. Ko and Raymond H. [illegible]

MAY 1991

(NASA-TM-4290) COMBINED COMPRESSIVE AND
SHEAR BUCKLING ANALYSIS OF HYPERSONIC
AIRCRAFT STRUCTURAL SANDWICH PANELS (NASA)
38 p CSCL 20K Unclas
H1/39 0019998

NASA Technical Memorandum 4290

Combined Compressive and Shear Buckling Analysis of Hypersonic Aircraft Structural Sandwich Panels

William L. Ko and Raymond H. Jackson
Ames Research Center
Dryden Flight Research Facility
Edwards, California

NASA
National Aeronautics and
Space Administration
Office of Management
Scientific and Technical
Information Division
1991

Dr. William L. Ko and the Dryden Flight Research Facility community would like to acknowledge the hard work and dedication of Raymond H. Jackson, whose recent death occurred during the final stages of this report. He and Dr. Ko were also completing several other reports prior to his death. Mr. Jackson contributed greatly to the programming of complicated mathematical equations for studying buckling behavior of structural panels for the National AeroSpace Plane.

CONTENTS

1 ABSTRACT 1

2 INTRODUCTION 1

3 NOMENCLATURE 1

4 HOT STRUCTURAL PANELS 3

5 BUCKLING ANALYSIS 5
- 5.1 Panel Constitutive Equations 5
- 5.2 Panel Boundary Conditions 6
- 5.3 Energy Equations 6
- 5.4 Rayleigh-Ritz Method 7

6 NUMERICAL RESULTS 10
- 6.1 Physical Properties of Panels 10
- 6.2 Convergency of Eigenvalue Solutions 12
- 6.3 Buckling Interaction Curves 14

7 CONCLUDING REMARKS 28

APPENDIX —FLEXURAL, TWISTING, AND TRANVERSE SHEAR STIFFNESSES 29

REFERENCES 32

1 ABSTRACT

The combined-load (compression and shear) buckling equations were established for orthotropic sandwich panels by using the Rayleigh-Ritz method to minimize the panel total potential energy. The resulting combined-load buckling equations were used to generate buckling interaction curves for super-plastically-formed/ diffusion-bonded titanium truss-core sandwich panels and titanium honeycomb-core sandwich panels having the same specific weight. The relative combined-load buckling strengths of these two types of sandwich panels are compared with consideration of their sandwich core orientations. For square and nearly square panels of both types, the combined load always induces symmetric buckling. As the panel aspect ratios increase, antisymmetric buckling will show up when the loading is shear-dominated combined loading. The square panel (either type) has the highest combined buckling strength, but the combined load buckling strength drops sharply as the panel aspect ratio increases. For square panels, the truss-core sandwich panel has higher compression-dominated combined-load buckling strength. However, for shear dominated loading, the square honeycomb-core sandwich panel has higher shear-dominated combined load buckling strength.

2 INTRODUCTION

Extensive explorative work has been carried out to find highly efficient (high stiffness, low specific weight) hot structural panel concepts for application to hypersonic flight vehicles such as the National AeroSpace Plane (NASP, refs. 1–12). The typical high-efficiency hot structural panels investigated hitherto are tubular and beaded panels (refs. 1–11) made of René 41, and sandwich panels with different core geometries, fabricated with superalloys (e.g., titanium, Inconel 617®, René 41). The face sheets of the sandwich panel may be either continous alloy or metal-matrix composites (e.g., silicon carbide/titanium metal-matrix composites, ref. 12).

During applications (or services), the hot structural panel will be subjected to combined loading induced by aerodynamic and thermal loadings. Therefore, the critical requirement for those hot structural panels is the high buckling strength. The buckling behavior of tubular and beaded panels has been studied extensively theoretically and experimentally (refs. 9–11). References 13 and 14 report some results of the compressive buckling behavior of truss-core and honeycomb-core sandwich panels.

Because these two types of sandwich panels could be good candidates for applications to the NASP, it is important to understand the relative structural performances of those two panels under the combined loadings. This report compares the buckling strengths of the truss-core and honeycomb-core sandwich panels of identical specific weight subjected to combined compressive and shear loadings.

3 NOMENCLATURE

A_{mn}	Fourier coefficient of trial function for w, in
a	length of sandwich panel, in
a_{mn}^{ij}	coefficients of characteristic equations
B_{mn}	Fourier coefficient of trial function for γ_x, rad
b	horizontal projected length of corrugation leg excluding the flat segments, in
C_{mn}	Fourier coefficient of trial function for γ_y, rad
c	width of sandwich panel, in

®Inconel is a registered trademark of Huntington Alloy Products Division, International Nickel Company, Huntington, WV.

D^*	flexural stiffness parameter, $\sqrt{\bar{D}_x \bar{D}_y}$, in-lb
D_{Qx}, D_{Qy}	transverse shear stiffnesses in planes parallel and normal to the corrugation axis (x-axis), lb/in-rad
D_x, D_y	longitudinal and transverse panel flexural stiffnesses, in-lb
$\bar{D}_x$, $\bar{D}_y$	panel flexural stiffnesses, in-lb
D_{xy}	panel twisting stiffness, in-lb
D_z^F, D_y^H, D_z^H	nondimensional parameters that are functions of truss-core geometric parameters
d	one half the length of straight diagonal segment of corrugation leg, in
E_c	Young's modulus of sandwich core material, lb/in^2
E_{cx}, E_{cy}, E_{cz}	effective Young's modulii of honeycomb core, lb/in^2
E_x, E_y	Young's modulii of face sheets, lb/in^2
f	length of flat horizontal region of corrugation leg, in
G_c	shear modulus of sandwich core material, lb/in^2
G_{cxy}, G_{cyz}, G_{czx}	effective shear modulii of honeycomb core, lb/in^2
G_{xy}	shear modulus of face sheets, lb/in^2
h	depth of sandwich panel = distance between middle planes of two face sheets, in
h_c	depth of corrugation = vertical distance between center lines of upper and lower flat segments of corrugation leg, $h_c = h - t_s - t_f$, in
h_c'	depth of honeycomb core, $h_c' = h - t_s$, in
I_c	moment of inertia, per unit width, of truss-core sheet of thickness t_c, $I_c = \frac{1}{12} t_c{}^3$, in^4/in
$\bar{I}_c$	moment of inertia, per unit width, of truss-core cross section taken with respect to the horizontal centroidal axis of the corrugation cross section, in^4/in
I_f	moment of inertia, per unit width, of corrugation leg flat region of thickness t_f, $I_f = \frac{1}{12} t_f{}^3$, in^4/in
I_s	moment of inertia, per unit width, of two face sheets, taken with respect to horizontal centroidal axis (neutral axis) of the sandwich panel, $I_s = \frac{1}{2} t_s h^2 + \frac{1}{6} t_s{}^3$, in^4/in
i	index, 1,2,3, . . .
j	index, 1,2,3, . . .
k_x	compressive buckling load factor, $k_x = \frac{N_x a^2}{\pi^2 D^*}$
k_{xy}	shear buckling load factor, $k_{xy} = \frac{N_{xy} a^2}{\pi^2 D^*}$
ℓ	length of corrugation leg, in
M_x, M_y	bending moment intensities, in-lb/in
M_{xy}	twisting moment intensities, in-lb/in

m	number of buckle half waves in x-direction
N_x, N_y	normal stress resultants, lb/in
N_{xy}	shear stress resultant, lb/in
n	number of buckle half waves in y-direction
p	one half of corrugation pitch = half wave length of corrugation, in
Q_x, Q_y	transverse shear force intensities, lb/in
R	radius of circular arc regions of corrugation leg, in
R_x	compressive stress ratio, $R_x = \frac{k_x}{k_x(\text{pure compression})}$
R_{xy}	shear stress ratio, $R_{xy} = \frac{k_{xy}}{k_{xy}(\text{pure shear})}$
$\bar{S}$	transverse shear stiffness parameter
t_c	thickness of straight diagonal segment, or circular arc regions of corrugation leg, $t_c = t_f \frac{p-f}{\ell - f}$, in
t_f	thickness of corrugation leg horizontal flat segments, in
t_s	thickness of sandwich face sheets, in
V	total potential energy of sandwich panel, in-lb
V_1	strain energy of the sandwich panel, in-lb
V_2	work done by external loads, in-lb
w	panel deflection, in
x, y, z	rectangular Cartesian coordinates
γ_x, γ_y	thickness shear strains, rad
δ_{mnij}	special delta function obeying $m \neq i$, $n \neq j$, $m \pm i = odd$, $n \pm j = odd$, $\delta_{mnij} = \frac{mnij}{(m^2 - i^2)(n^2 - j^2)}$
θ	corrugation angle, rad
ν_c	Poisson ratio of sandwich core material
ν_{cxy}, ν_{cyz}, ν_{cxz}	Poisson ratios of honeycomb core
ν_{xy}, ν_{yx}	Poisson ratios of face sheets, also for sandwich panel
ρ_{HC}	specific weight of honeycomb core, lb/in^3
ρ_{Ti}	specific weight of titanium material, lb/in^3

4 HOT STRUCTURAL PANELS

Figures 1 and 2 show titanium truss-core and honeycomb-core sandwich panels, respectively. The truss-core sandwich panel may be fabricated by a superplastical-forming/diffusion-bonding process. The honeycomb-core sandwich panel can be fabricated by an enhanced-diffusion bonding process which joins the two face sheets to the honeycomb core (ref. 12). To compare the buckling strength, both types of the sandwich panels have the same face sheet thickness and same core depth. The thickness of the truss is adjusted so that the two types of panels will have identical specific weight. The sandwich panels will be subjected to combined compressive and shear loadings as shown in figure 3. For each type of panel, two cases of core orientations will be investigated. Namely, truss-core orientation,

case 1 = corrugation axis parallel to N_x and
case 2 = corrugation axis perpendicular to N_x;

honeycomb-core orientation,
case 1 = hexagon longitudinal axis parallel to N_x and
case 2 = hexagon longitudinal axis perpendicular to N_x.

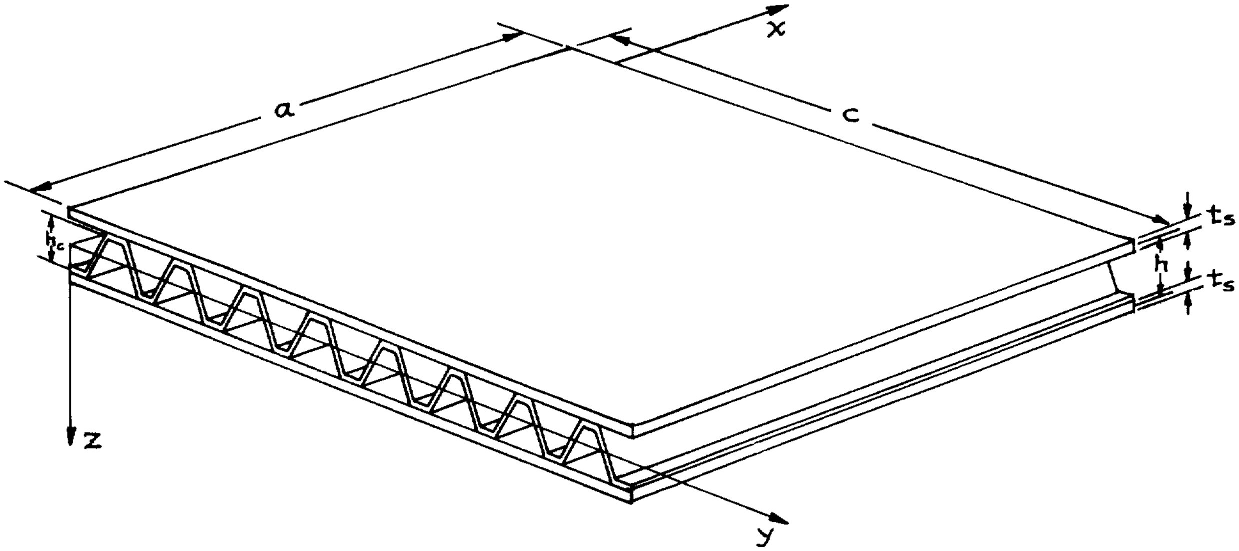

Figure 1. Truss-core sandwich panel.

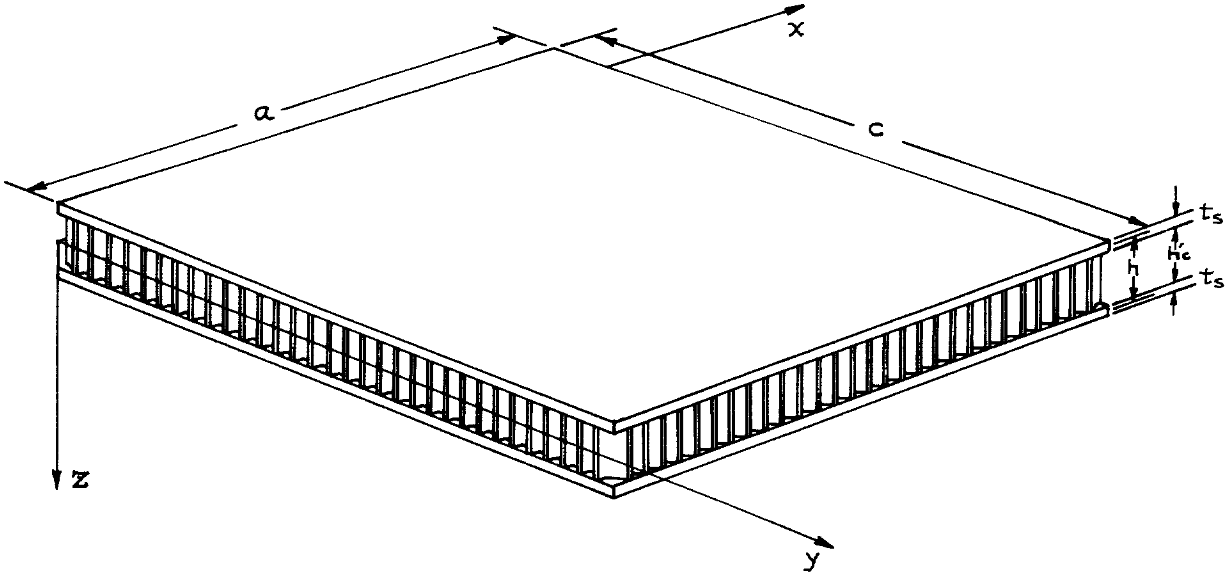

Figure 2. Honeycomb-core sandwich panel.

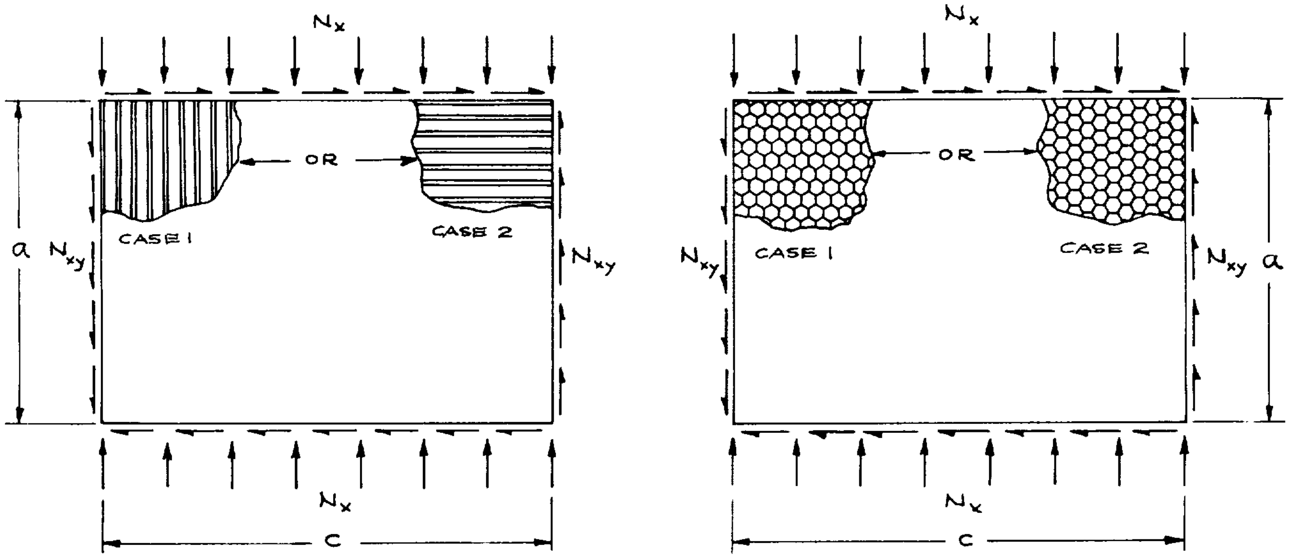

Figure 3. Truss-core and honeycomb-core sandwich panels of the same specific weight under compression and shear.

5 BUCKLING ANALYSIS

5.1 Panel Constitutive Equations

The sandwich panel constitutive equations (moment and shear equations, ref. 15) may be expressed as

$$M_x = -\frac{D_x}{1-\nu_{xy}\nu_{yx}}\left[\frac{\partial}{\partial x}\left(\frac{\partial w}{\partial x}-\gamma_x\right)+\nu_{yx}\frac{\partial}{\partial y}\left(\frac{\partial w}{\partial y}-\gamma_y\right)\right] \tag{1}$$

$$M_y = -\frac{D_y}{1-\nu_{xy}\nu_{yx}}\left[\frac{\partial}{\partial y}\left(\frac{\partial w}{\partial y}-\gamma_y\right)+\nu_{xy}\frac{\partial}{\partial x}\left(\frac{\partial w}{\partial x}-\gamma_x\right)\right] \tag{2}$$

$$M_{xy} = \frac{D_{xy}}{2}\left[\frac{\partial}{\partial x}\left(\frac{\partial w}{\partial y}-\gamma_y\right)+\frac{\partial}{\partial y}\left(\frac{\partial w}{\partial x}-\gamma_x\right)\right] \tag{3}$$

$$Q_x = D_{Qx}\,\gamma_x \tag{4}$$

$$Q_y = D_{Qy}\,\gamma_y \tag{5}$$

where M_x and M_y are the bending moment intensities, M_{xy} is the twisting moment intensity, Q_x and Q_y are the intensities of transverse shear resultants (fig. 4), w is the panel deflection, γ_x and γ_y are the transverse shear strains, ν_{xy} and ν_{yx} are the panel Poisson ratios, D_x and D_y are the flexural stiffnesses, D_{xy} is the twisting stiffness, and D_{Qx} and D_{Qy} are the transverse shear stiffnesses. D_x, D_y, D_{xy}, D_{Qx}, and D_{Qy} are defined in the appendix.

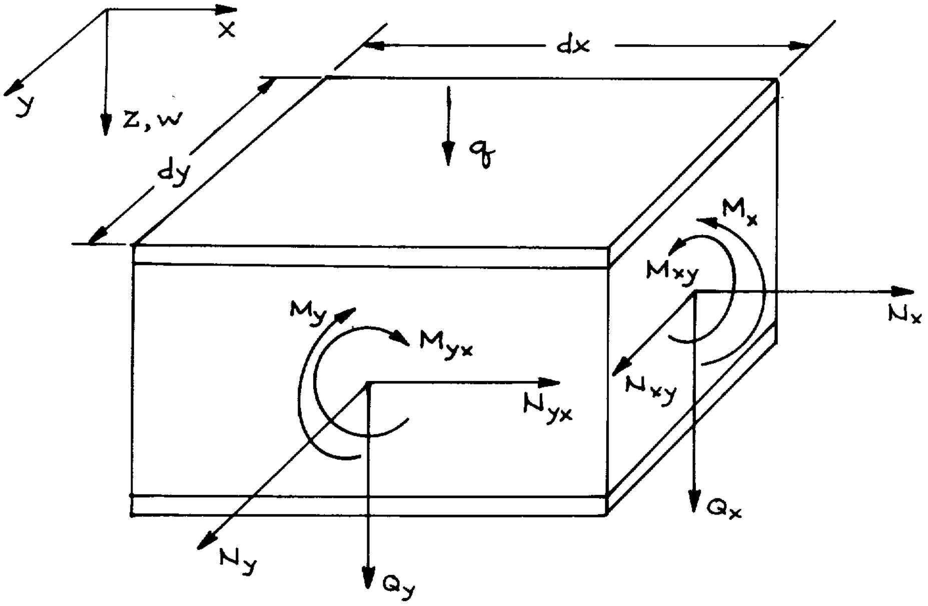

Figure 4. Forces and moments acting on a differential element of a sandwich panel.

5.2 Panel Boundary Conditions

The sandwich panels will be assumed to be simply supported at four edges. Namely

$$w = M_x = \gamma_y = 0 \quad \text{along} \quad x = 0, a \tag{6}$$

$$w = M_y = \gamma_x = 0 \quad \text{along} \quad x = 0, c \tag{7}$$

5.3 Energy Equations

The strain energy V_1 produced by the moments M_x, M_y, M_{xy} ($= M_{yx}$), and the transverse shear forces Q_x and Q_y (fig. 4) may be written as (ref. 15)

$$\begin{aligned} V_1 = \frac{1}{2}\int_0^a \int_0^c \Bigg\{ & \frac{D_x}{1-\nu_{xy}\nu_{yx}} \left[\frac{\partial}{\partial x}\left(\frac{\partial w}{\partial x} - \gamma_x\right)\right]^2 \\ & + \frac{D_x \nu_{yx} + D_y \nu_{xy}}{1-\nu_{xy}\nu_{yx}} \left[\frac{\partial}{\partial x}\left(\frac{\partial w}{\partial x} - \gamma_x\right)\right] \left[\frac{\partial}{\partial y}\left(\frac{\partial w}{\partial y} - \gamma_y\right)\right] \\ & \times \frac{D_y}{1-\nu_{xy}\nu_{yx}} \left[\frac{\partial}{\partial y}\left(\frac{\partial w}{\partial y} - \gamma_y\right)\right]^2 + \frac{D_{xy}}{2} \left[\frac{\partial}{\partial x}\left(\frac{\partial w}{\partial y} - \gamma_y\right) + \frac{\partial}{\partial y}\left(\frac{\partial w}{\partial x} - \gamma_x\right)\right]^2 \\ & + D_{Qx}\gamma_x^2 + D_{Qy}\gamma_y^2 \Bigg\} dx dy \end{aligned} \tag{8}$$

and the strain energy V_2 produced by the external loads N_x, N_y, N_{xy}, and q can be expressed as (ref. 15)

$$V_2 = \frac{1}{2}\int_0^a \int_0^c \left[-2qw + N_x\left(\frac{\partial w}{\partial x}\right)^2 + N_y\left(\frac{\partial w}{\partial y}\right)^2 + 2N_{xy}\frac{\partial w}{\partial x}\frac{\partial w}{\partial y}\right] dx dy \tag{9}$$

Then, the total potential energy V of the sandwich system is given

$$V = V_1 + V_2 \tag{10}$$

For the present problem, $q = N_y = 0$, and $N_x \rightarrow -N_x$.

5.4 Rayleigh-Ritz Method

Because of the existence of the shear loading term $N_{xy} \frac{\partial w}{\partial x} \frac{\partial w}{\partial y}$ appearing in equation (9), the Rayleigh-Ritz method will be used to minimize the total potential energy V of the sandwich system to obtain the buckling equation for combined loading.

To satisfy the simply-supported boundary conditions equations (6) and (7), the following trial functions for the panel deflection w and the transverse shear strains γ_x and γ_y may be chosen (ref. 16)

$$w = \sum_{m=1}^{\infty} \sum_{n=1}^{\infty} A_{mn} \sin \frac{m\pi x}{a} \sin \frac{n\pi y}{c} \tag{11}$$

$$\gamma_x = \sum_{m=1}^{\infty} \sum_{n=1}^{\infty} B_{mn} \cos \frac{m\pi x}{a} \sin \frac{n\pi y}{c} \tag{12}$$

$$\gamma_y = \sum_{m=1}^{\infty} \sum_{n=1}^{\infty} C_{mn} \sin \frac{m\pi x}{a} \cos \frac{n\pi y}{c} \tag{13}$$

where A_{mn}, B_{mn}, and C_{mn} are the undetermined Fourier coefficients of the assumed trial functions for w, γ_x, and γ_y respectively, and m and n are the buckle half wave numbers in the x and y direction. Substitution of equations (11) through (13) into equations (8) and (9) and then substitution of the resulting expressions of V_1 and V_2 into equation (10), and applying the Rayleigh principle of minimizing V

$$\frac{\partial V}{\partial A_{mn}} = \frac{\partial V}{\partial B_{mn}} = \frac{\partial V}{\partial C_{mn}} = 0 \tag{14}$$

one obtains three simultaneous characteristic equations for the determination of the combined buckling loads.

For $\frac{\partial V}{\partial A_{mn}} = 0$

$$\left(a_{mn}^{11} - k_x \frac{m^2 \pi^4}{a^4} \right) A_{mn} + 32 \frac{\pi^2 k_{xy}}{a^3 c} \sum_{i=1}^{\infty} \sum_{j=1}^{\infty} \delta_{mnij} A_{ij} + a_{mn}^{12} B_{mn} + a_{mn}^{13} C_{mn} = 0 \tag{15}$$

For $\frac{\partial V}{\partial B_{mn}} = 0$

$$a_{mn}^{21} A_{mn} + a_{mn}^{22} B_{mn} + a_{mn}^{23} C_{mn} = 0 \tag{16}$$

For $\frac{\partial V}{\partial C_{mn}} = 0$

$$a_{mn}^{31} A_{mn} + a_{mn}^{32} B_{mn} + a_{mn}^{33} C_{mn} = 0 \tag{17}$$

In equation (15), the buckling load factors k_x and k_{xy} are respectively defined as

$$k_x = \frac{N_x a^2}{\pi^2 D^*} \quad , \quad k_{xy} = \frac{N_x a^2}{\pi^2 D^*} \tag{18}$$

where the flexural stiffness parameter D^* is defined as

$$D^* = \frac{\sqrt{E_x E_y}}{1 - \nu_{xy} \nu_{yx}} I_s \tag{19}$$

In addition, the special delta function δ_{mnij} appearing in equation (15) is defined as

$$\delta_{mnij} = \frac{mnij}{(m^2 - i^2)(n^2 - j^2)} \tag{20}$$

which obeys the conditions: $m \neq i$, $n \neq i$, $m \pm i = \text{odd}$, $n \pm j = \text{odd}$.

The coefficients a^{ij}_{mn} $(i, j = 1, 2, 3)$ appearing in equations (15) through (17) are defined as follows

$$a^{11}_{mn} = \bar{D}_x \left(\frac{m\pi}{a}\right)^4 + (\bar{D}_x \nu_{yx} + \bar{D}_y \nu_{xy} + 2\,D_{xy}) \left(\frac{m\pi}{a}\right)^2 \left(\frac{n\pi}{c}\right)^2 + \bar{D}_y \left(\frac{n\pi}{c}\right)^4 \tag{21}$$

$$a^{12}_{mn} = a^{21}_{mn} = -\left[\bar{D}_x \left(\frac{m\pi}{a}\right)^3 + \frac{1}{2}(\bar{D}_x \nu_{yx} + \bar{D}_y \nu_{xy} + 2\,D_{xy}) \left(\frac{m\pi}{a}\right) \left(\frac{n\pi}{c}\right)^2\right] \tag{22}$$

$$a^{13}_{mn} = a^{31}_{mn} = -\left[\bar{D}_y \left(\frac{n\pi}{c}\right)^3 + \frac{1}{2}(\bar{D}_x \nu_{yx} + \bar{D}_y \nu_{xy} + 2\,D_{xy}) \left(\frac{m\pi}{a}\right)^2 \left(\frac{n\pi}{c}\right)\right] \tag{23}$$

$$a^{22}_{mn} = \bar{D}_x \left(\frac{m\pi}{a}\right)^2 + \frac{D_{xy}}{2} \left(\frac{n\pi}{c}\right)^2 + D_{Qx} \tag{24}$$

$$a^{23}_{mn} = a^{32}_{mn} = \frac{1}{2}(\bar{D}_x \nu_{yx} + \bar{D}_y \nu_{xy} + D_{xy}) \left(\frac{m\pi}{a}\right) \left(\frac{n\pi}{c}\right) \tag{25}$$

$$a^{33}_{mn} = \bar{D}_y \left(\frac{n\pi}{c}\right)^2 + \frac{D_{xy}}{2} \left(\frac{m\pi}{a}\right)^2 + D_{Qy} \tag{26}$$

In the previous

$$\bar{D}_x = \frac{D_x}{1 - \nu_{xy}\nu_{yx}} \quad , \quad \bar{D}_y = \frac{D_y}{1 - \nu_{xy}\nu_{yx}} \tag{27}$$

Solving for B_{mn} and C_{mn} in terms of A_{mn} from equations (16) and (17), one obtains

$$B_{mn} = \frac{a^{23}_{mn} a^{31}_{mn} - a^{21}_{mn} a^{33}_{mn}}{a^{22}_{mn} a^{33}_{mn} - a^{23}_{mn} a^{32}_{mn}} A_{mn} \tag{28}$$

$$C_{mn} = \frac{a^{21}_{mn} a^{32}_{mn} - a^{22}_{mn} a^{31}_{mn}}{a^{22}_{mn} a^{33}_{mn} - a^{23}_{mn} a^{32}_{mn}} A_{mn} \tag{29}$$

Substitution of equations (28) and (29) into equation (15) yields a homogenous linear equation containing only the panel deflection coefficient A_{mn}

$$\frac{M_{mn}}{k_{xy}} A_{mn} + \sum_{i=1}^{\infty} \sum_{j=1}^{\infty} \delta_{mnij} A_{ij} = 0 \tag{30}$$

where $m \neq i$, $n \neq j$, $m \pm i = \text{odd}$, $n \pm i = \text{odd}$, and

$$M_{mn} = \frac{ac}{32} \left\{ k_x \left(\frac{m\pi}{a}\right)^2 - \frac{a^2}{\pi^2 D^*} \left[\underset{\substack{\uparrow \\ \text{classical thin} \\ \text{plate theory term}}}{a^{11}_{mn}} + \underbrace{\frac{a^{12}_{mn}(a^{23}_{mn} a^{31}_{mn} - a^{21}_{mn} a^{33}_{mn}) + a^{13}_{mn}(a^{21}_{mn} a^{32}_{mn} - a^{22}_{mn} a^{31}_{mn})}{a^{22}_{mn} a^{33}_{mn} - a^{23}_{mn} a^{32}_{mn}}}_{\text{transverse sheer effect terms}} \right] \right\} \tag{31}$$

Equation (30) forms a system of an infinite number of simultaneous equations associated with different values of m and n. For practical purposes, the number of these simultaneous equations may be cut off up to certain finite numbers if the convergency of the eigenvalue solutions reached the desired limit. Since $m \pm n =$ odd and $n \pm j$ = odd is required in equation (20), we have $(m \pm i) \pm (n \pm j) = (m \pm n) \pm (i \pm j)$ = even. Thus, if $m \pm n =$ even, then $(i \pm j)$ must also be even. Likewise, if $m \pm n =$ odd, then $(i \pm j)$ must also be odd. Therefore, there is no coupling between even case and odd case in each equation written out from equation (30) for a particular set of {m,n}. Namely, if the A_{mn} term in equation (30) is for $m \pm n =$ even (or odd), then the A_{ij} term in the same equation must be for $(i \pm j)$ = even (or odd) also. Thus, the simultaneous equations generated from equation (30) may be divided into two groups which are independent of each other; one group in which $m \pm n$ is even (i.e., symmetrical buckling), and the other in which $m \pm n$ is odd (i.e., antisymmetrical buckling, refs. 17, 18). For the deflection coefficients A_{mn} to have nontrivial solutions for given values of k_x and $\frac{c}{a}$, the determinant of the coefficients of the unknown A_{mn} must vanish. The largest eigenvalue $\frac{1}{k_{xy}}$ thus obtained will give the lowest buckling load factor k_{xy} as a function of k_x and $\frac{c}{a}$. Thus, a family of buckling interaction curves in the k_x–k_{xy} space may be generated with $\frac{c}{a}$ as a parameter. Representative characteristic equations (buckling equations) for 12 × 12 matrices written out from equation (30) are shown respectively in equations (32) and (33) for the cases $m \pm n =$ even and $m \pm n =$ odd (refs. 17, 18).

$m \pm n =$ even

$$\begin{array}{r|cccccccccccc|}
 & A_{11} & A_{13} & A_{22} & A_{31} & A_{15} & A_{24} & A_{33} & A_{42} & A_{51} & A_{35} & A_{44} & A_{53} \\
m=1,n=1 & \frac{M_{11}}{k_{xy}} & 0 & \frac{4}{9} & 0 & 0 & \frac{8}{45} & 0 & \frac{8}{45} & 0 & 0 & \frac{16}{225} & 0 \\
m=1,n=3 & & \frac{M_{13}}{k_{xy}} & -\frac{4}{5} & 0 & 0 & \frac{8}{7} & 0 & -\frac{8}{25} & 0 & 0 & \frac{16}{35} & 0 \\
m=2,n=2 & & & \frac{M_{22}}{k_{xy}} & -\frac{4}{5} & -\frac{20}{63} & 0 & \frac{36}{25} & 0 & -\frac{20}{63} & \frac{4}{7} & 0 & \frac{4}{7} \\
m=3,n=1 & & & & \frac{M_{31}}{k_{xy}} & 0 & -\frac{8}{25} & 0 & \frac{8}{7} & 0 & 0 & \frac{16}{35} & 0 \\
m=1,n=5 & & & & & \frac{M_{15}}{k_{xy}} & -\frac{40}{27} & 0 & -\frac{8}{63} & 0 & 0 & -\frac{16}{27} & 0 \\
m=2,n=4 & & & & & & \frac{M_{24}}{k_{xy}} & -\frac{72}{35} & 0 & -\frac{8}{63} & \frac{8}{3} & 0 & -\frac{120}{147} \\
m=3,n=3 & & & \text{Symmetry} & & & & \frac{M_{33}}{k_{xy}} & -\frac{72}{35} & 0 & 0 & \frac{144}{49} & 0 \\
m=4,n=2 & & & & & & & & \frac{M_{42}}{k_{xy}} & -\frac{40}{27} & -\frac{120}{147} & 0 & \frac{8}{3} \\
m=5,n=1 & & & & & & & & & \frac{M_{51}}{k_{xy}} & 0 & -\frac{16}{27} & 0 \\
m=3,n=5 & & & & & & & & & & \frac{M_{35}}{k_{xy}} & -\frac{80}{21} & 0 \\
m=4,n=4 & & & & & & & & & & & \frac{M_{44}}{k_{xy}} & -\frac{80}{21} \\
m=5,n=3 & & & & & & & & & & & & \frac{M_{53}}{k_{xy}}
\end{array} = 0 \tag{32}$$

where the nonzero off-diagonal terms satisfy the conditions: $m \neq i, n \neq j, m \pm i$ = odd and $n \pm j$ = odd.

$m \pm n = \text{odd}$

$$\begin{array}{r|cccccccccccc|l}
 & A_{12} & A_{21} & A_{14} & A_{23} & A_{32} & A_{41} & A_{16} & A_{25} & A_{34} & A_{43} & A_{52} & A_{61} & \\
m=1,n=2 & \frac{M_{12}}{k_{xy}} & -\frac{4}{9} & 0 & \frac{4}{5} & 0 & -\frac{8}{45} & 0 & \frac{20}{63} & 0 & \frac{8}{25} & 0 & -\frac{4}{35} & \\
m=2,n=1 & & \frac{M_{21}}{k_{xy}} & -\frac{8}{45} & 0 & \frac{4}{5} & 0 & -\frac{4}{35} & 0 & \frac{8}{25} & 0 & \frac{20}{63} & 0 & \\
m=1,n=4 & & & \frac{M_{14}}{k_{xy}} & -\frac{8}{7} & 0 & -\frac{16}{225} & 0 & \frac{40}{27} & 0 & -\frac{16}{35} & 0 & -\frac{8}{175} & \\
m=2,n=3 & & & & \frac{M_{23}}{k_{xy}} & -\frac{36}{25} & 0 & -\frac{4}{9} & 0 & \frac{72}{35} & 0 & -\frac{4}{7} & 0 & \\
m=3,n=2 & & & & & \frac{M_{32}}{k_{xy}} & -\frac{8}{7} & 0 & -\frac{4}{7} & 0 & \frac{72}{35} & 0 & -\frac{4}{9} & \\
m=4,n=1 & & & & & & \frac{M_{41}}{k_{xy}} & -\frac{8}{175} & 0 & -\frac{16}{35} & 0 & \frac{40}{27} & 0 & = 0 \\
m=1,n=6 & & & \text{Symmetry} & & & & \frac{M_{16}}{k_{xy}} & -\frac{20}{11} & 0 & -\frac{8}{45} & 0 & -\frac{36}{1225} & \\
m=2,n=5 & & & & & & & & \frac{M_{25}}{k_{xy}} & -\frac{8}{3} & 0 & -\frac{100}{441} & 0 & \\
m=3,n=4 & & & & & & & & & \frac{M_{34}}{k_{xy}} & -\frac{144}{49} & 0 & -\frac{8}{45} & \\
m=4,n=3 & & & & & & & & & & \frac{M_{43}}{k_{xy}} & -\frac{8}{3} & 0 & \\
m=5,n=2 & & & & & & & & & & & \frac{M_{52}}{k_{xy}} & -\frac{20}{11} & \\
m=6,n=1 & & & & & & & & & & & & \frac{M_{61}}{k_{xy}} &
\end{array} \tag{33}$$

where the nonzero off-diagonal terms satisfy the conditions: $m \neq i$, $n \neq j$, $m \pm i = \text{odd}$ and $n \pm j = \text{odd}$.

Notice that the diagonal terms in the determinants (eq. (32), (33)) come from the first term of equation (30), and the second series term of equation (30) gives the off-diagonal terms of the determinants.

6 NUMERICAL RESULTS

6.1 Physical Properties of Panels

The titanium truss-core and titanium honeycomb-core sandwich panels analyzed have the following geometrical and material properties.

Geometry:

Items	Truss-core sandwich panel	Honeycomb-core sandwich panel
a, in	24	24
$b = \frac{1}{2}(p - f)$, in	0.3294	---
$\frac{c}{a}$	1, 2, 3, 4	1, 2, 3, 4
$d = \frac{b}{\cos\theta}$, in	0.6589	---
f, in	0	---
h, in	1.2	1.2
$h_c = h - t_s - t_f$, in	1.1412	---
$h_c' = h - t_s$, in	---	1.1680
$\ell = f + 2(d + R\theta)$, in	1.3177	---
$p = \frac{h_c}{\tan\theta}$, in	0.6589	---
R, in	0	---
$t_c = t_f \cos\theta$, in	0.0134	---
t_f, in	0.0268	---
t_s, in	0.0320	0.0320
θ, deg	60	---

Material properties

The titanium material used for the sandwich panel face sheets and cores has the following properties

$$E_x = E_y = E_c = 16 \times 10^6 \text{lb/in}^2$$

$$G_{xy} = G_c = 6.2 \times 10^6 \text{lb/in}^2$$

$$\nu_{xy} = \nu_{yx} = \nu_c = 0.31$$

$$\rho_{Ti} = 0.16 \text{ lb/in}^3$$

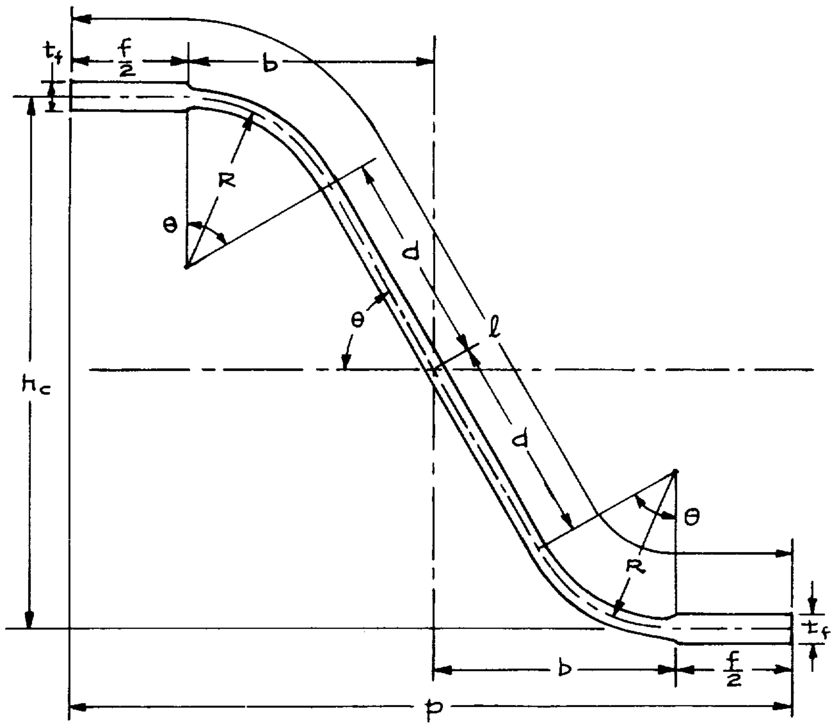

Figure 5. Corrugation leg of a truss core.

The effective elastic constants used for the titanium honeycomb cores are given in the following

For case 1 core orientation

$$E_{cx} = 2.7778 \times 10^4 \text{lb/in}^2$$

$$E_{cy} = 2.7778 \times 10^4 \text{lb/in}^2$$

$$E_{cz} = 2.7778 \times 10^5 \text{lb/in}^2$$

$$G_{cxy} = 0.00613 \text{ lb/in}^2$$

$$G_{cyz} = 0.81967 \times 10^5 \text{lb/in}^2$$

$$G_{czx} = 1.81 \times 10^5 \text{lb/in}^2$$

$$\nu_{cxy} = 0.658 \times 10^{-2}$$

$$\nu_{cyz} = 0.643 \times 10^{-6}$$

$$\nu_{cxz} = 0.643 \times 10^{-6}$$

$$\rho_{HC} = 3.674 \times 10^{-3} \text{lb/in}^3$$

For case 2 core orientation: subscripts x and y are interchanged.

6.2 Convergency of Eigenvalue Solutions

To find the minimum number of simultaneous equations (written out from eq. (30)) required to yield sufficiently accurate eigenvalue solutions, the order of determinants (eq. (32) and (33)) was gradually increased from order 4 until the eigenvalues sufficiently converged. Figure 6, which is the plots of table 1, shows the convergency behavior of k_{xy} (even and odd) with the increase of the order of matrices for a special case of $k_x = 0$ and $\frac{c}{a} = 1$, for truss-core sandwich panel of case 1 core orientation.

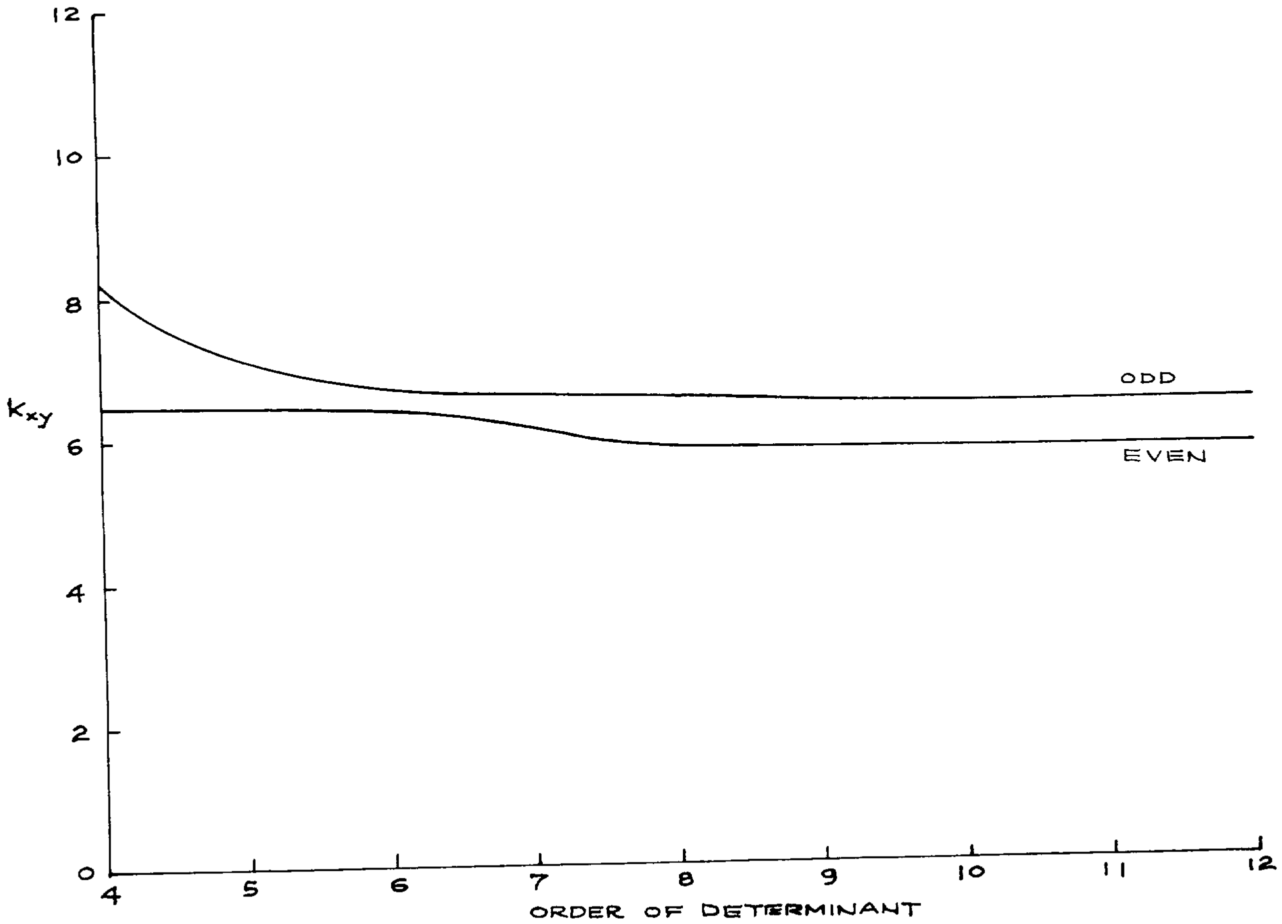

Figure 6. Convergency of shear buckling solutions with an increase of the order of matrix. $k_x = 0$, $\frac{c}{a} = 1$.

Table 1. Convergency of k_{xy} for truss-core sandwich panel of case 1 core orientation.

Order of determinant	k_{xy}, even	k_{xy}, odd
4	6.43	8.19
6	6.39	6.64
8	5.79	6.58
10	5.76	6.34
12	5.72	6.33

The values of k_{xy} (even and odd) have sufficiently converged at order 12. Thus, in the actual calculations of k_{xy} for any given values of k_x and $\frac{c}{a}$, the order of matrices was set to be 12 (eq. (32) and (33)).

6.3 Buckling Interaction Curves

Figures 7 through 10 show buckling interaction curves for the truss-core and honeycomb-core sandwich panels of the same specific weight and of different core orientations, respectively. Both symmetric and antisymmetric buckling cases are shown for different aspect ratios of the panels. For the square panels ($\frac{c}{a} = 1$), the antisymmetic buckling interaction curves (broken curves) lay on the right hand side of the symmetric buckling interaction curves without intersecting. For $\frac{c}{a} \geq 2$, the symmetric and antisymmetric curves intersect at certain combined loading points at the shear dominated combined loading region. Figure 11 shows the comparison of the composite buckling interaction curves for the two types of sandwich panels. Those composite buckling interaction curves were constructed from figures 7 through 10 by combining portions of symmetric and antisymmetric buckling interaction curves to give minimum combined buckling loads. For square panels ($\frac{c}{a} = 1$) (any type), the core orientation has no effect on the pure compressive and pure shear buckling strength of the panels, and has negligible effect on the combined-load buckling strength of the panels. When the aspect ratio is increased, the effect of core orientation becomes conspicuous. For square panels ($\frac{c}{a} = 1$), the truss-core sandwich panels (any core orientation) have higher buckling strength than the honeycomb-core sandwich panels (any core orientation) when the loading is compression dominated combined loading. When the loading is shear dominated, the latter has the higher buckling strength. For an aspect ratio greater than 1, the two cases of interaction curves of honeycomb-core sandwich panel practically lay between the two interaction curves for the truss-core sandwich panel. Figure 12 shows k_x plotted as a function of $\frac{c}{a}$ for the two types of sandwich panels.

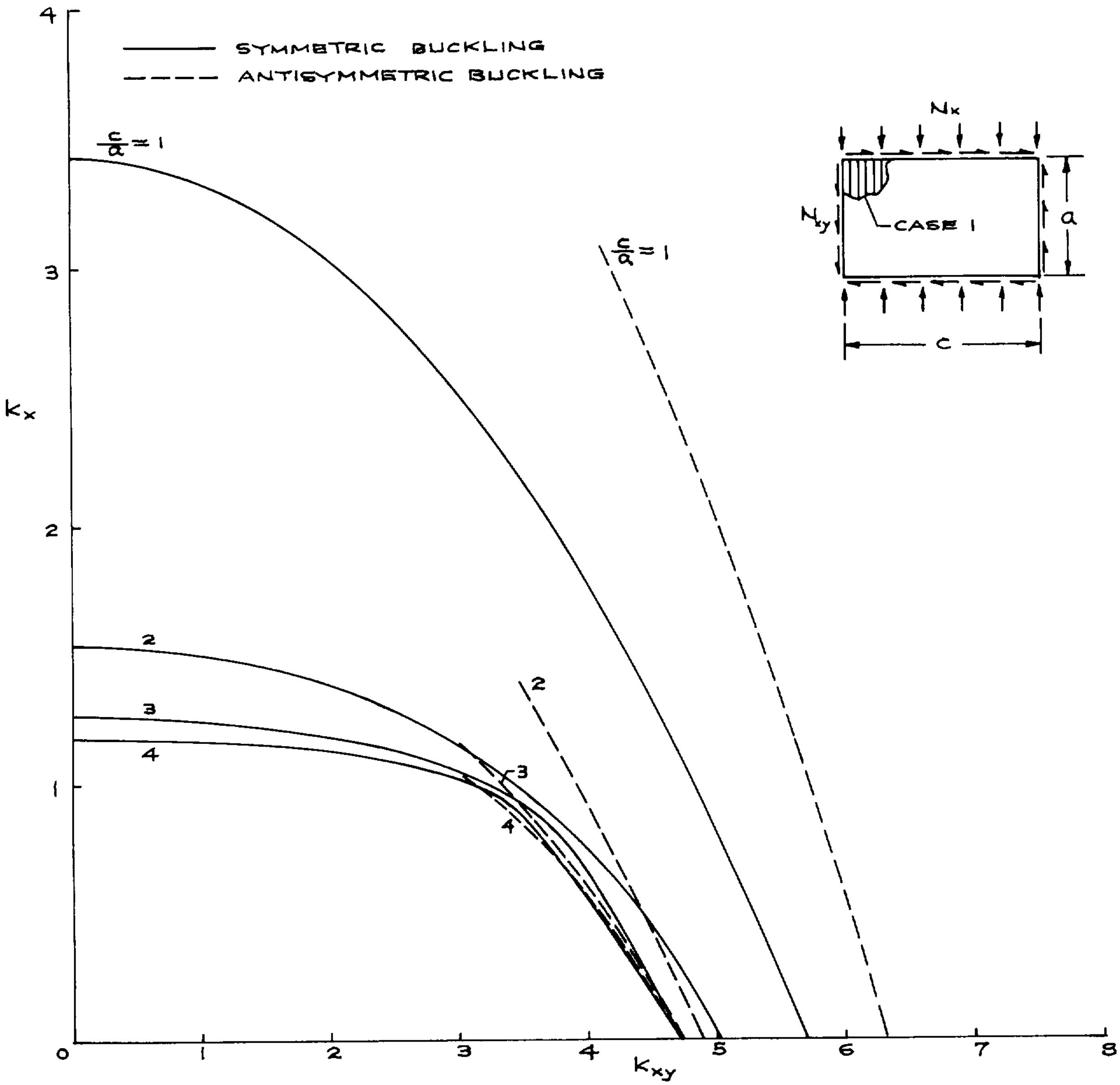

Figure 7. Buckling interaction plots for truss-core sandwich panels of different aspect ratios. N_x is parallel to the corrugation axis.

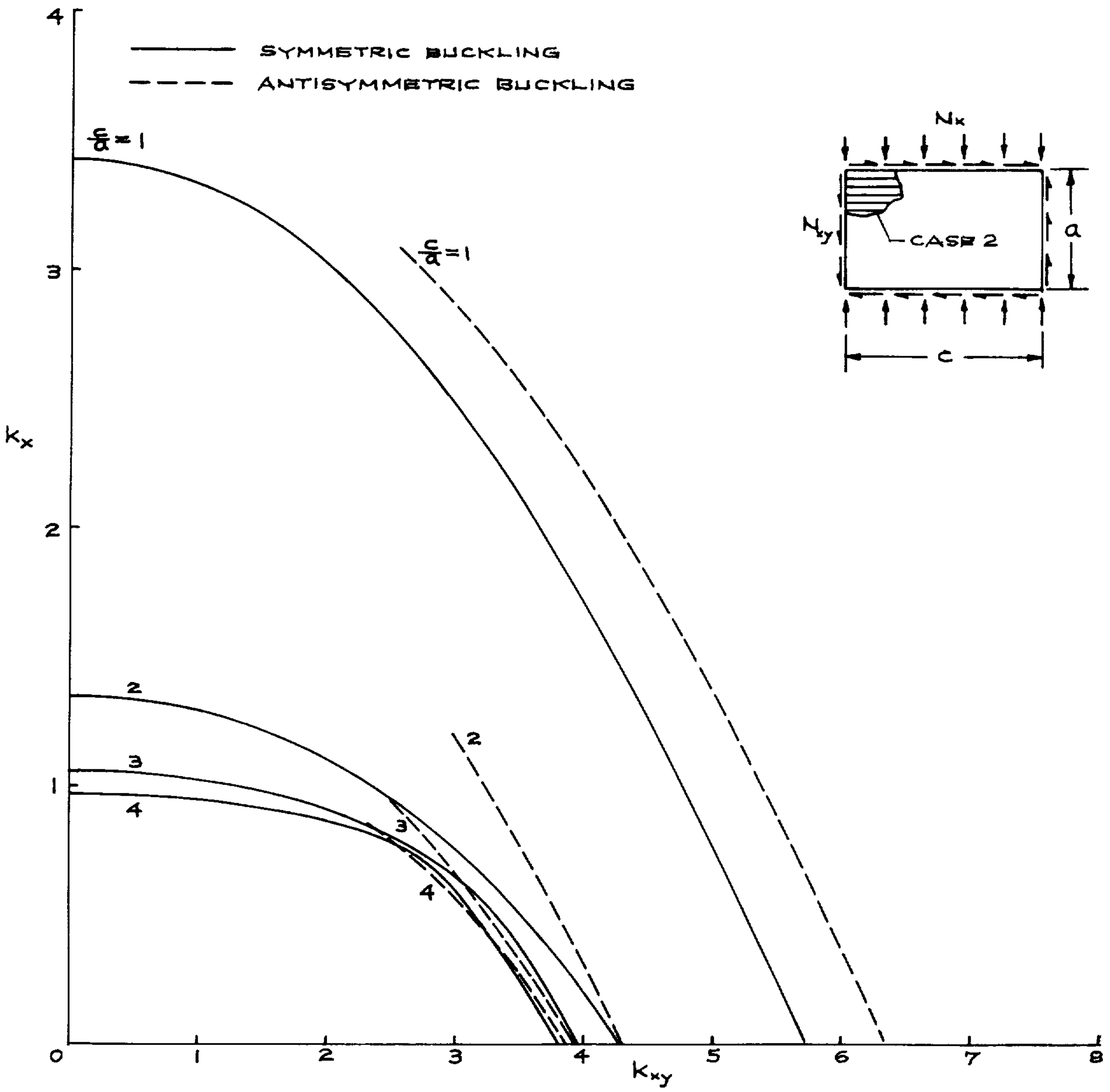

Figure 8. Buckling interaction plots for truss-core sandwich panels of different aspect ratios. N_x is perpendicular to the corrugation axis.

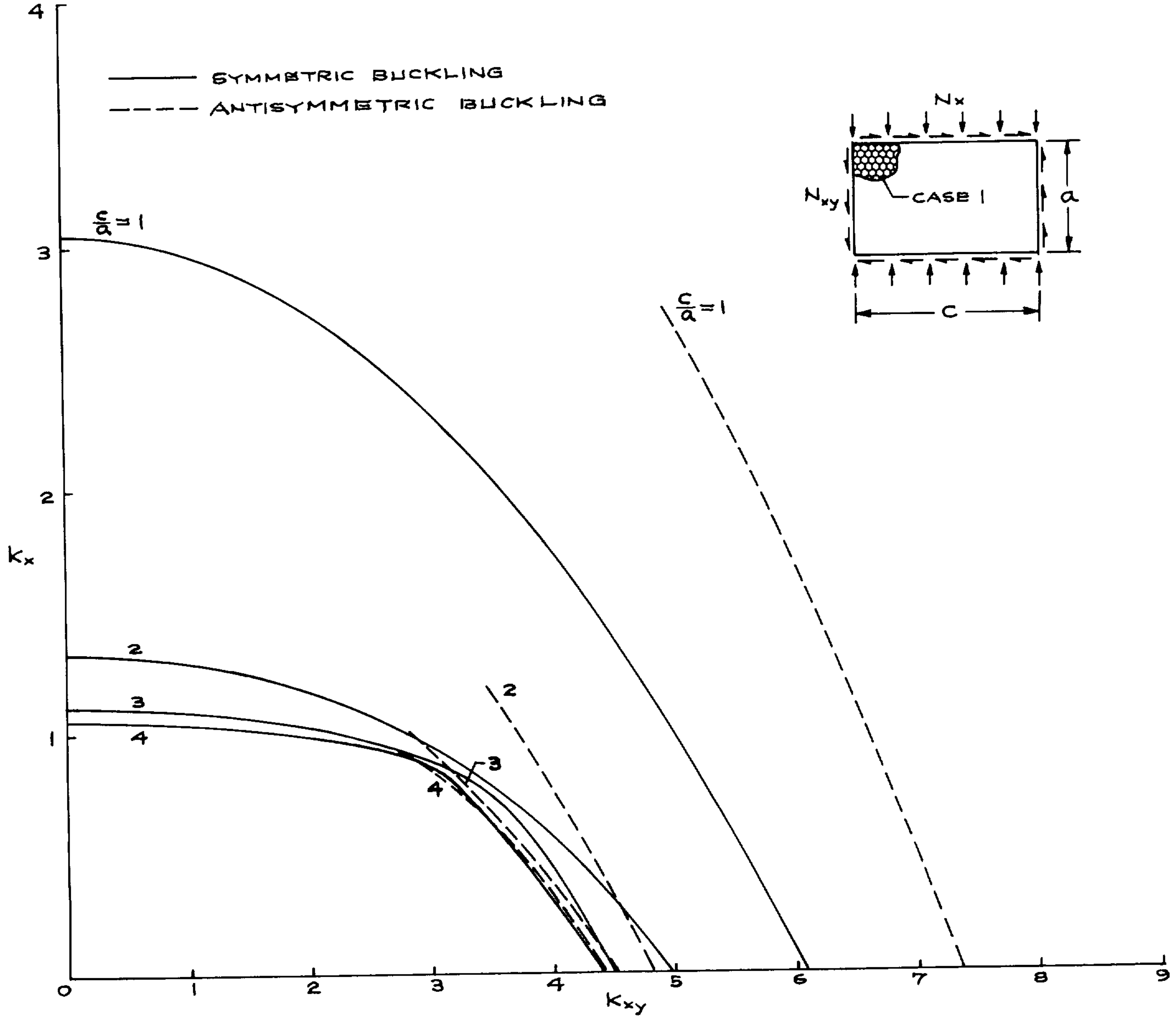

Figure 9. Buckling interaction plots for honeycomb-core sandwich panels of different aspect ratios. Case 1 core orientation.

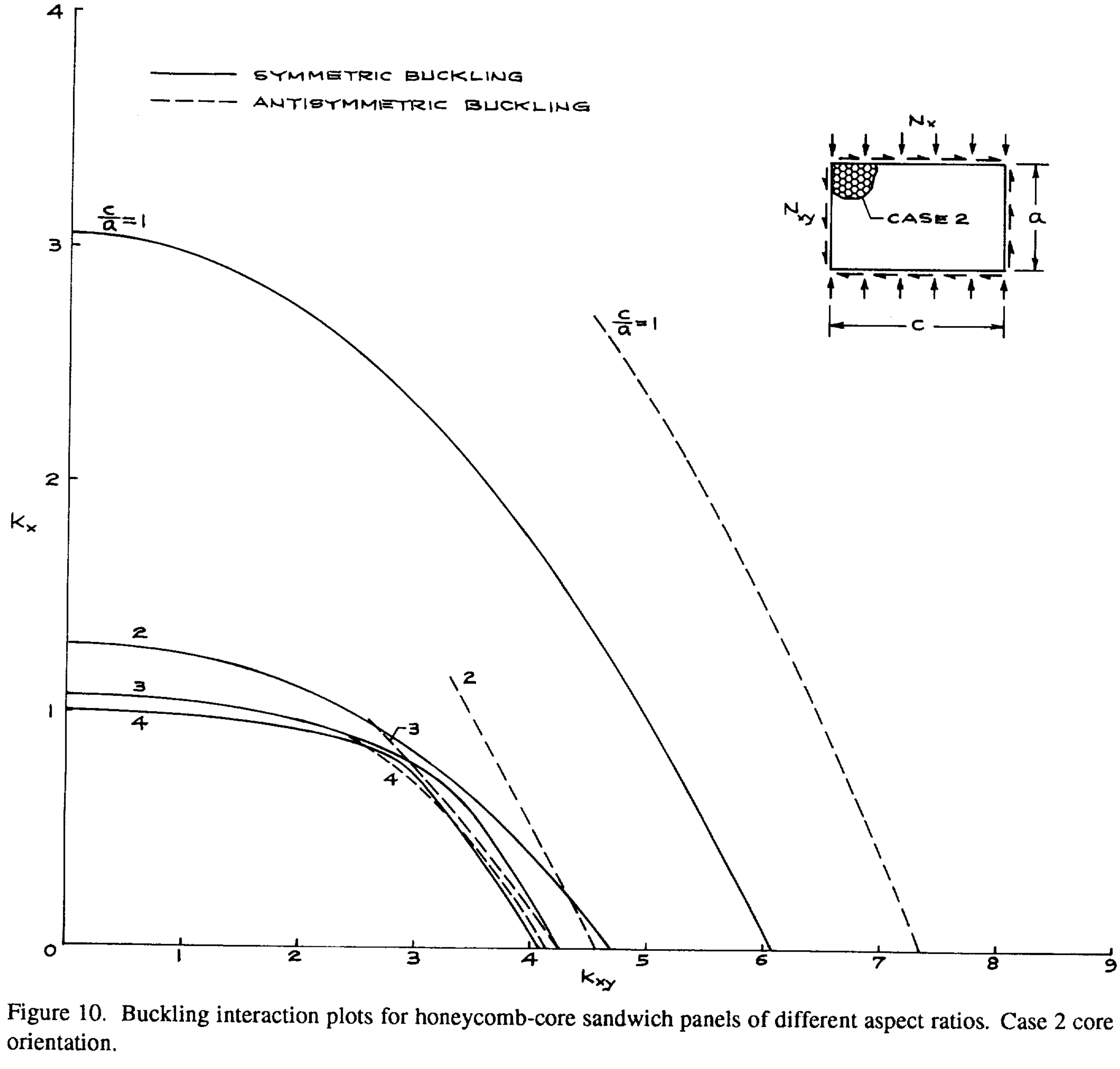

Figure 10. Buckling interaction plots for honeycomb-core sandwich panels of different aspect ratios. Case 2 core orientation.

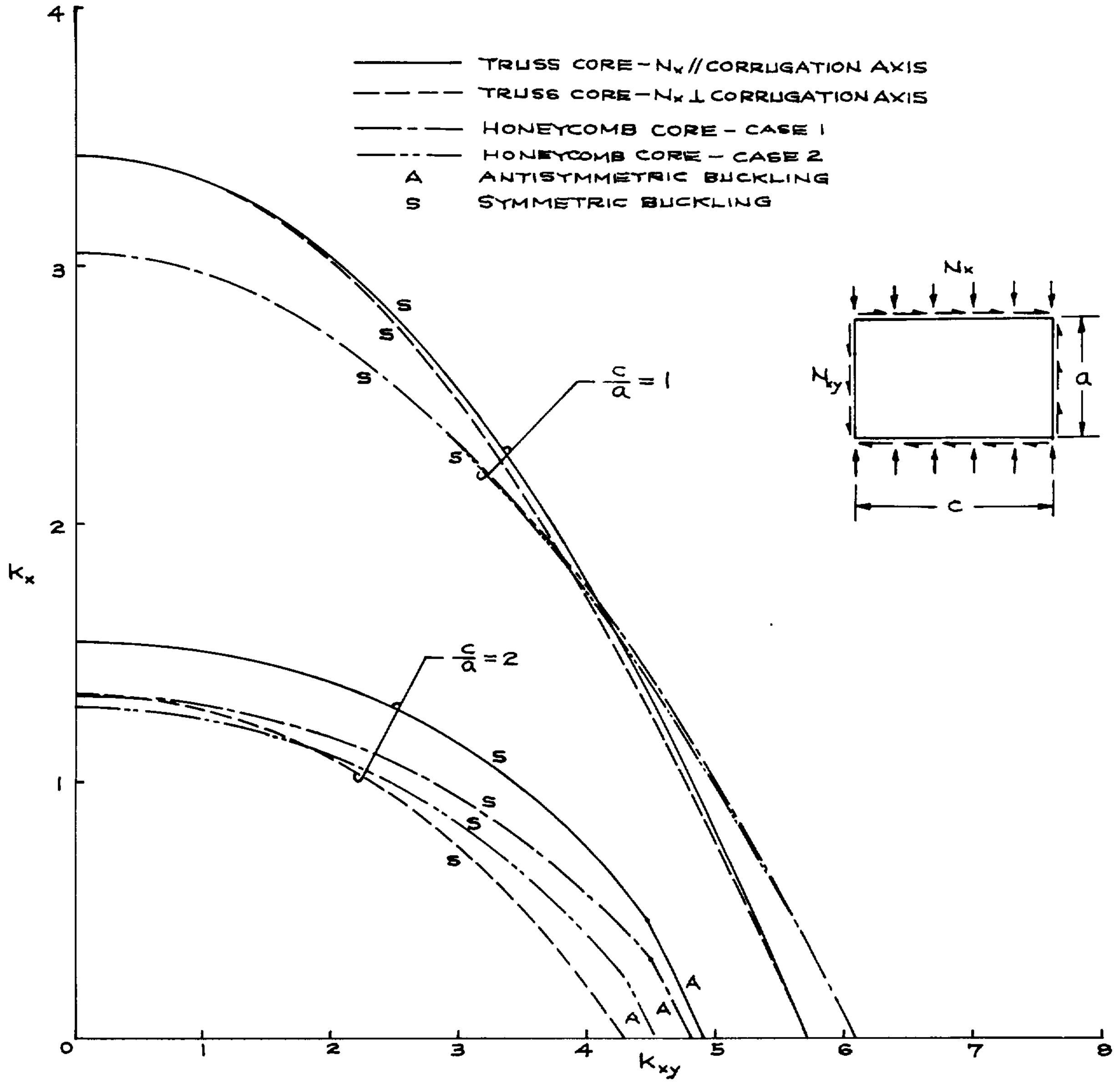

Figure 11(a). Comparison of buckling strength of truss-core and honeycomb-core sandwich panels having the same specific weight.

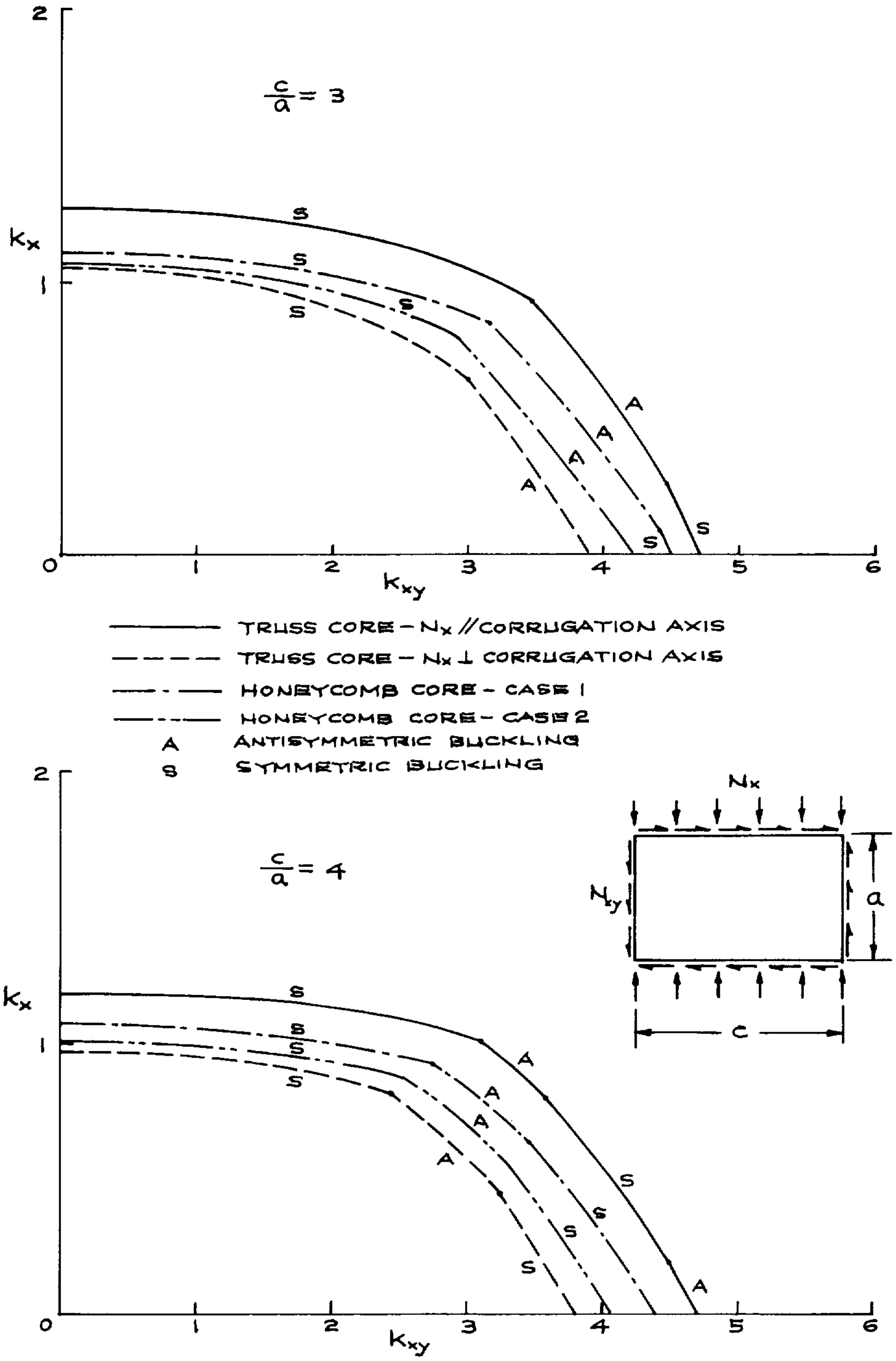

Figure 11(b). Concluded.

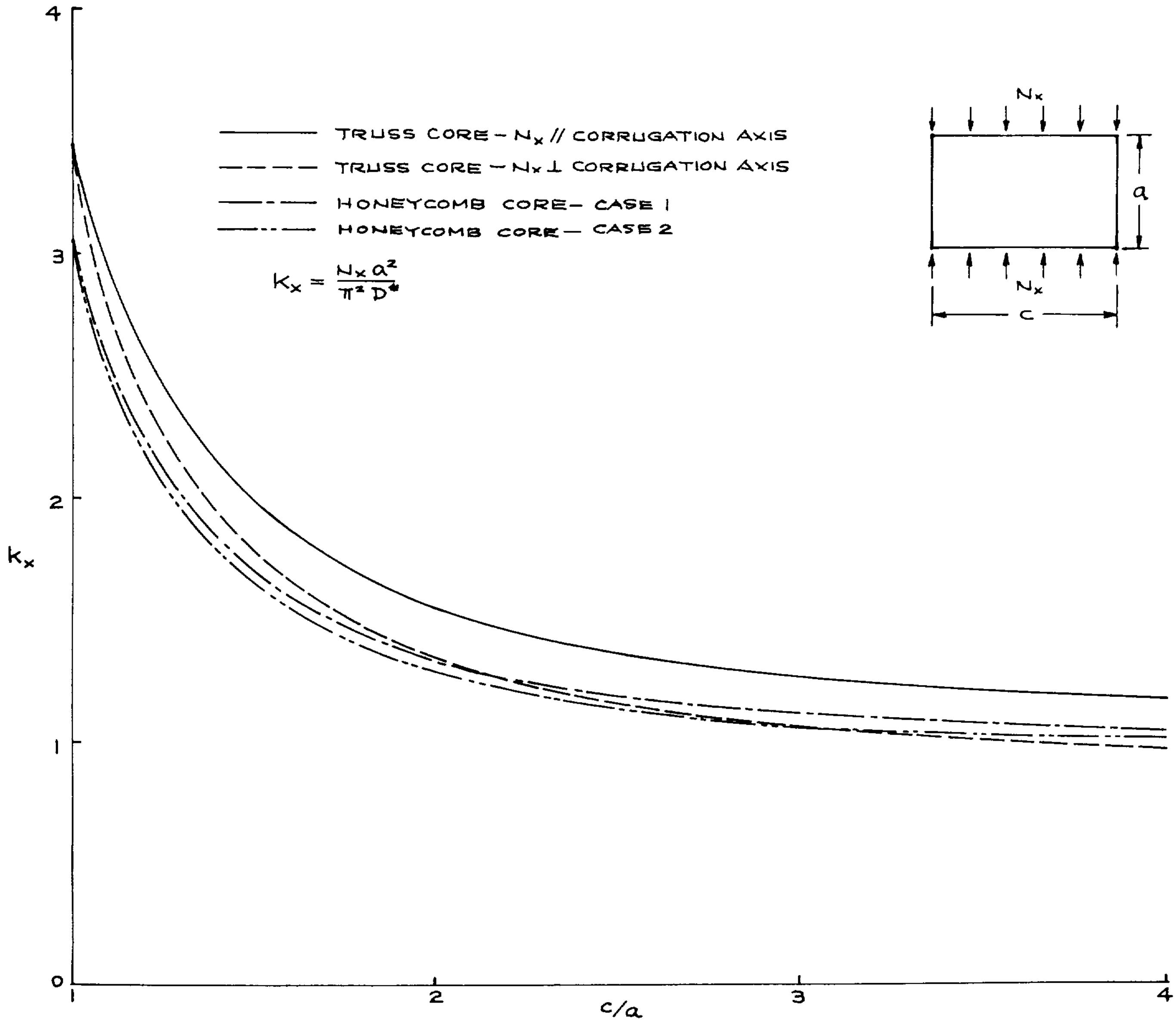

Figure 12. Comparison of compressive buckling strength of truss-core and honeycomb-core sandwich panels having the same specific weight.

It is seen that the value of k_x decreases sharply as the aspect ratio $\frac{c}{a}$ is increased from $\frac{c}{a} = 1$ to $\frac{c}{a} = 2$. Beyond $\frac{c}{a} = 2$, the rate of decrease of k_x with the increase in $\frac{c}{a}$ becomes less severe. For compressive buckling strength, the truss-core sandwich panel of case 1 core orientation has a higher value of k_x than the honeycomb-core sandwich panel for all the range of panel aspect ratio $\frac{c}{a}$. For case 2 core orientation, the former has a higher value of k_x than the latter only up to $\frac{c}{a} \approx 2.1$. Figure 13 shows similar plots for k_{xy}. The rate of decrease of k_{xy} with the increase in $\frac{c}{a}$ is less severe as compared with the compressive buckling case (fig. 12). The honeycomb-core sandwich panel has higher shear buckling strength only in the range of aspect ratio $1 < \frac{c}{a} < 1.5$(case 1 core orientation) or $1 < \frac{c}{a} < 1.25$(case 2 core orientation). Beyond $\frac{c}{a} = 1.5$, the truss-core sandwich panel with case 1 core orientation has higher shear buckling strength. Table 2 summarizes the values of k_x and k_{xy} for different panel aspects ratios.

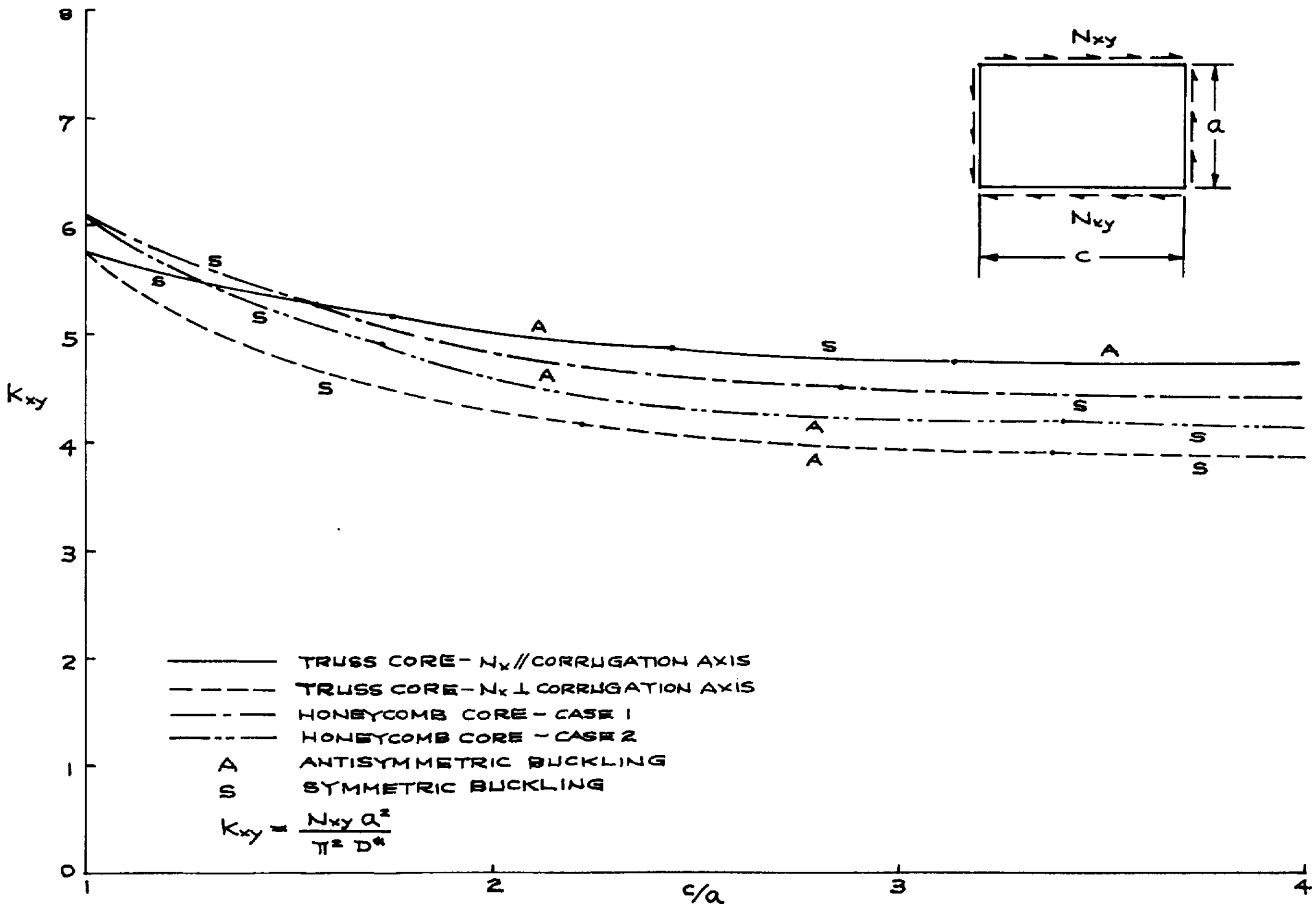

Figure 13. Comparison of shear buckling strength of truss-core and honeycomb-core sandwich panels having the same specific weight.

Table 2. Buckling load factors for truss-core and honeycomb-core sandwich panels having same specific weight.

	k_x				k_{xy} (symmetric)				k_{xy} (antisymmetric)			
	Truss-core sandwich panel		Honeycomb-core sandwich panel		Truss-core sandwich panel		Honeycomb-core sandwich panel		Truss-core sandwich panel		Honeycomb-core sandwich panel	
$\frac{c}{a}$	case 1	case 2	case1	case 2	case1	case 2	case 1	case 2	case 1	case 2	case 1	case 2
1	3.4321	3.4321	3.0529	3.0529	5.7160	5.7160	6.0831	6.0834	6.3284	6.3284	7.3575	7.3575
2	1.5533	1.3450	1.3351	1.2943	5.0279	4.2812	4.9674	4.6761	4.9106	4.3001	4.8060	4.5747
3	1.2724	1.0620	1.1177	1.0788	4.7186	3.9598	4.5042	4.2364	4.7496	3.9186	4.5115	4.2163
4	1.1799	0.9709	1.0495	1.0117	4.7497	3.8200	4.4070	4.0988	4.7148	3.8605	4.4279	4.1417

Figures 14 through 17 show the buckling interaction curves plotted in the stress-ratio spaces for the truss-core and honeycomb-core sandwich panels of different core orientations, respectively. For the aspect ratios $\frac{c}{a} = 1, 2$, the buckling interaction curves for the two types of panels are continuous curves. However, for $\frac{c}{a} = 3, 4$, the buckling interaction curves in figures 14 through 17 are discontinuous composite curves constructed from symmetric and antisymmetric buckling interaction curves. Those buckling interaction curves in the stress-ratio space for the two types of sandwich panels may be described by the following mathematical equations shown in table 3.

Table 3. Equations for describing buckling interaction curves in stress-ratio space.

	Truss-core sandwich panel		Honeycomb-core sandwich panel	
$\frac{c}{a}$	case 1	case 2	case 1	case 2
1	$R_x + R_{xy}^{2.04} \approx 1$	$R_x + R_{xy}^{1.92} \approx 1$	$R_x + R_{xy}^{2.00} \approx 1$	$R_x + R_{xy}^{1.98} \approx 1$
2	$R_x + R_{xy}^{2.86} \approx 1$	$R_x + R_{xy}^{2.29} \approx 1$	$R_x + R_{xy}^{2.52} \approx 1$	$R_x + R_{xy}^{2.39} \approx 1$
3	Discontinuous curve	Discontinuous curve	Discontinuous curve	Discontinuous curve
4	Discontinuous curve	Discontinuous curve	Discontinuous curve	Discontinuous curve

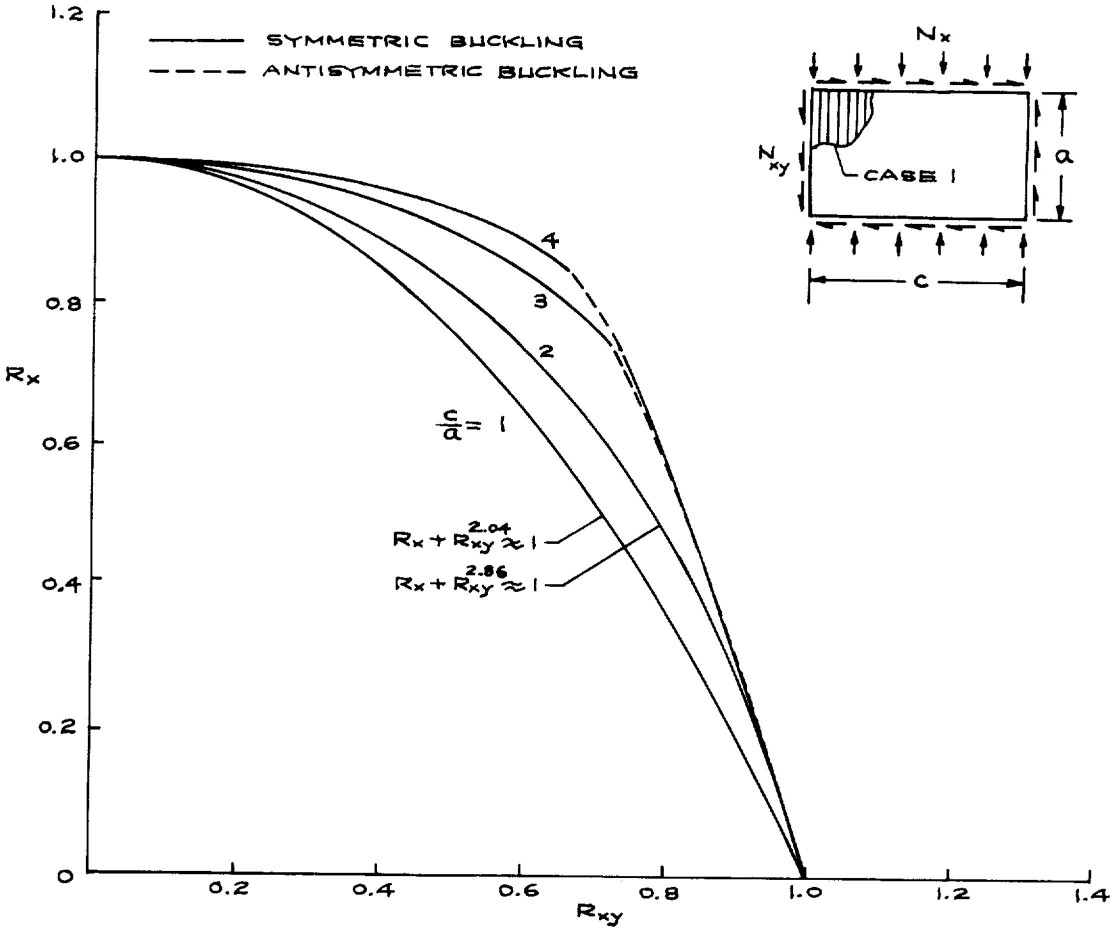

Figure 14. Buckling interaction plots in stress ratio space for truss-core sandwich panels of different aspect ratios. N_x is parallel to the corrugation axis.

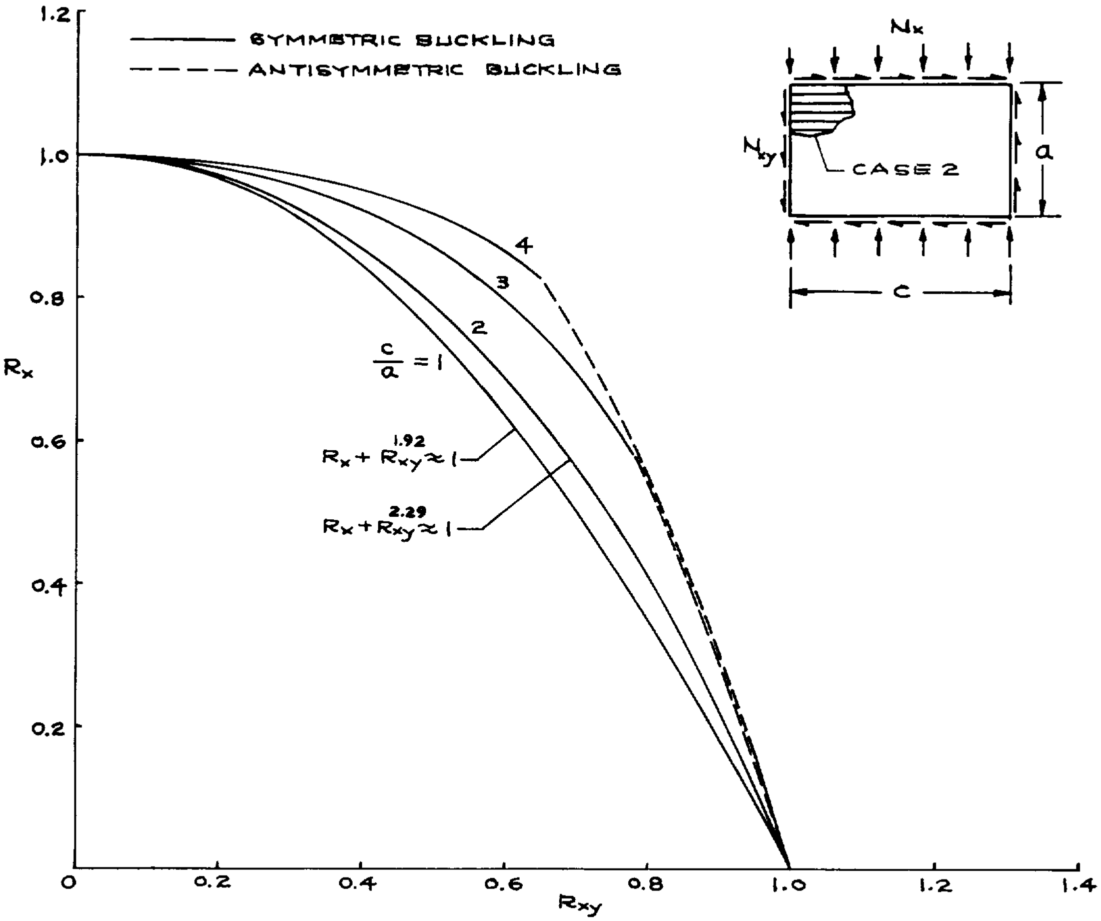

Figure 15. Buckling interaction plots in stress ratio space for truss-core sandwich panels of different aspect ratios. N_x is perpendicular to the corrugation axis.

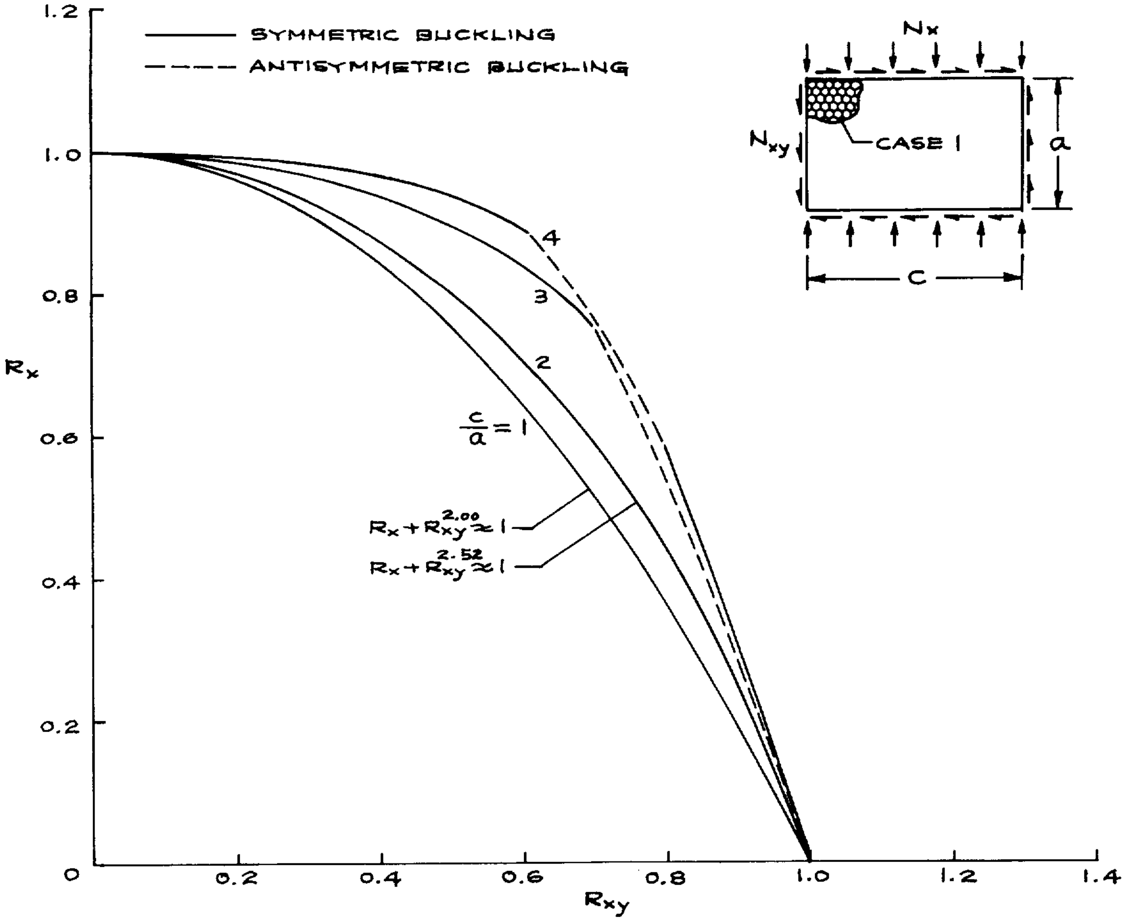

Figure 16. Buckling interaction plots in stress ratio space for honeycomb-core sandwich panels of different aspect ratios. Case 1 core orientation.

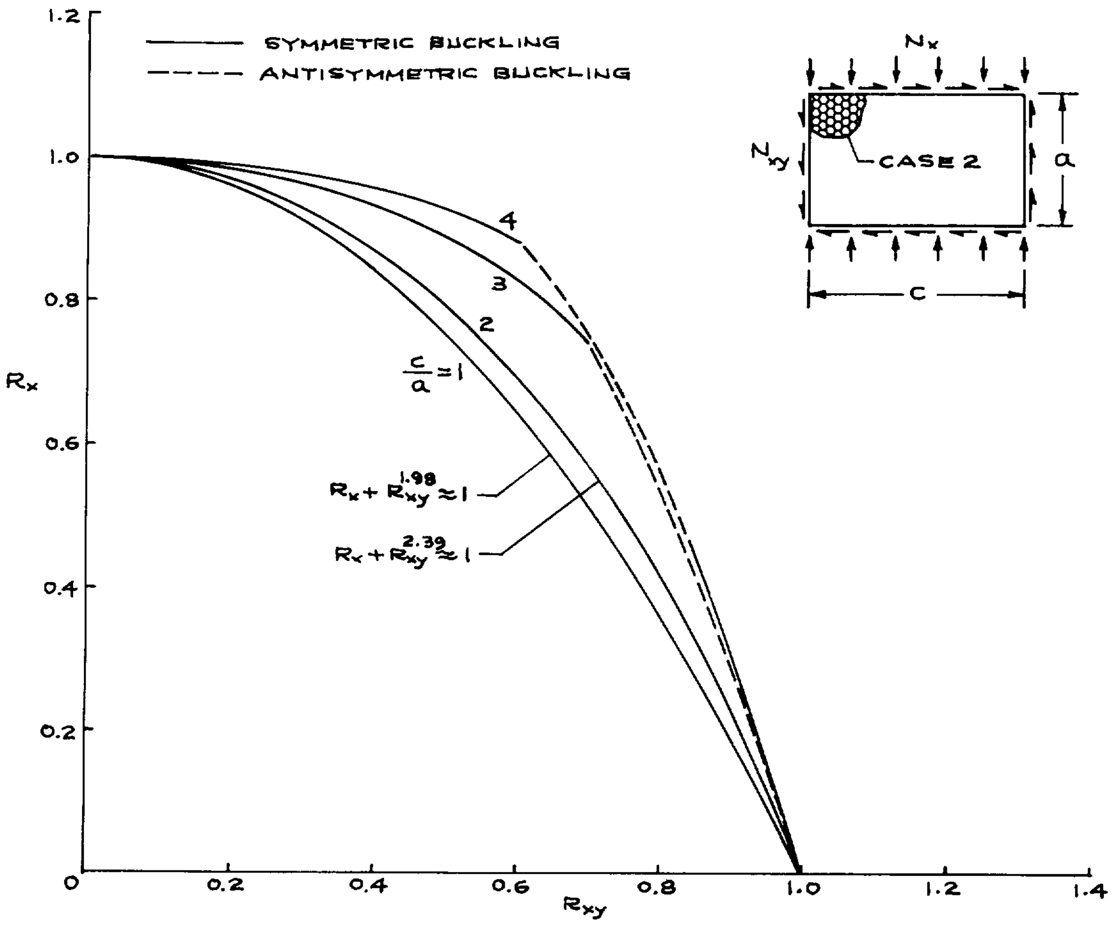

Figure 17. Buckling interaction plots in stress ratio space for honeycomb-core sandwich panels of different aspect ratios. Case 2 core orientation.

7 CONCLUDING REMARKS

Combined-load buckling analysis was performed on the truss-core and honeycomb-core sandwich panels having the same specific weight, and the combined-load buckling interaction curves were generated for these two types of sandwich panels with different panel aspect ratios and different core orientations. The results of the analysis are summarized in the following

1. The infinite number of simultaneous characteristic equations for calculating the shear buckling load components could be cut off at 12 (i.e., order of matrix 12) to yield sufficiently accurate eigenvalue solutions for shear buckling loads.

2. For square sandwich panels of both types, only the symmetric buckling will take place. For a panel aspect ratio greater than one, both symmetric and antisymmetric bucklings will take place. The antisymmetric buckling will occur when the combined loading is shear dominated.

3. The buckling interaction curves in the stress ratio space for both types of sandwich panels are continuous curves for low-panel aspect ratios, but become discontinuous composite curves at higher panel aspect ratios.

4. The square-shaped sandwich panel (any type) has the highest combined-load buckling strength, and the combined-load buckling strength decreases sharply as the panel aspect ratio is increased.

5. For a square sandwich panel (any type) the core orientation has no effect on pure compressive and pure shear buckling strength, but has negligible effect on the combined-load buckling strength. When the panel aspect ratio is increased, the effect of core orientation on the combined-load buckling strength becomes conspicuous.

6. For square sandwich panels, the truss-core sandwich panels (two core orientations) have higher buckling strength than the honeycomb-core sandwich panels (two core orientations) when the combined loading is compression dominated. The reverse is true when the combined loading is shear dominated.

7. For an aspect ratio greater than one, the two buckling interaction curves of honeycomb-core sandwich panels of two core orientations practically lay between the two buckling interaction curves of truss-core sandwich panels of two core orientations.

APPENDIX

FLEXURAL, TWISTING, AND TRANVERSE SHEAR STIFFNESSES

The flexural stiffnesses D_x and D_y, the twisting stiffness D_{xy}, and the transverse shear stiffnesses D_{Qx} and D_{Qy} of the truss-core and honeycomb-core sandwich panels are written in the following for anisotropic face sheet material and isotropic core material.

Truss-core sandwich panel, case 1 core orientation

$$D_x = E_x I_s + E_c \bar{I}_c \tag{A-1}$$

$$D_y = E_y I_s \frac{1 + \frac{E_c \bar{I}_c}{E_y I_s}}{1 + (1 - \nu_{xy}\nu_{yx}) \frac{E_c \bar{I}_c}{E_y I_s}} \tag{A-2}$$

$$D_{xy} = 2 G_{xy} I_s \tag{A-3}$$

$$D_{Qx} = \frac{G_c t_c h^2}{p\ell} \tag{A-4}$$

$$D_{Qy} = \bar{S} h \frac{E_c}{1 - \nu_c^2} \left(\frac{t_c}{h_c} \right)^3 \tag{A-5}$$

In the above equations, $\{E_x, E_y, G_{xy}, \nu_{xy}, \nu_{yx}\}$ and $\{E_c, G_c, \nu_c\}$ are the elastic constants associated, respectively, with the anisotropic face sheet material and the isotropic truss-core material, h is the depth of the sandwich panel, p is one half of the corrugation pitch, t_s is the thickness of the upper and lower face sheets, t_c is the final thickness of the core sheet after superplastic expansion and is related to the original core sheet thickness t_f through (figs. 1, 5)

$$t_c = t_f \frac{p - f}{\ell - f} \xrightarrow[f=0]{} t_f \cos\theta \tag{A-6}$$

where f is the length of corrugation leg horizontal flat segment, θ is the corrugation angle, and h_c in equation (A-5) is the depth of the corrugation defined as

$$h_c = h - (t_s + t_f) \tag{A-7}$$

and finally, ℓ is the length of corrugation leg expressed as

$$\ell = f + 2(d + R\theta) \tag{A-8}$$

where d is one half the length of the corrugation leg diagonal segment, and R is the radius of the circular arc segments of the corrugation leg (fig. 5).

In equations (A-1) and (A-2), I_s is the moment of inertia of the face sheets taken with respect to the centroidal axis of the sandwich panel, and $\bar{I}_c$ is the moment of inertia of the corrugation leg taken with respect to the corrugation core centroidal axis (parallel to y axis). The expressions for I_s and $\bar{I}_c$ are given in the following

$$I_s = \frac{1}{2} t_s h^2 + \frac{1}{6} t_s^3 \tag{A-9}$$

$$\begin{aligned} \bar{I}_c = \frac{h_c^3 t_c}{p} \Bigg\{ & \frac{1}{4} \frac{f}{h_c} \frac{t_f}{t_c} \left(1 + \frac{1}{3} \frac{t_c^2}{h_c^2} \right) + \frac{2}{3} \frac{d^3}{h_c^3} \left(\sin^2\theta + \frac{1}{4} \frac{t_c^2}{d^2} \cos^2\theta \right) \\ & + \frac{R}{h_c} \left[\frac{\theta}{2} - \frac{R^2}{h_c^2} \sin\theta (1 - \cos\theta) - \frac{R}{h_c} \left(2 - 3\frac{R}{h_c} \right) (\theta - \sin\theta) \right] \Bigg\} \end{aligned} \tag{A-10}$$

The nondimensional shear stiffness coefficient $\bar{S}$ appearing in equation (A-5) is defined as (refs. 13, 19)

$$\bar{S} = \frac{6\frac{h_c}{p}D_z^F\frac{t_s}{t_c} + \left(\frac{p}{h_c}\right)^2}{12\left\{\frac{h}{h_c}\frac{p}{h_c}D_z^F - 2\left(\frac{p}{h_c}\right)^2 D_z^H + \frac{h_c}{h}\left[6\frac{t_s}{t_c}\left(D_z^F D_y^H - D_z^{H^2}\right) + \left(\frac{p}{h_c}\right)^3 D_y^H\right]\right\}} \tag{A-11}$$

where the nondimensional parameters D_z^F, D_z^H, and D_y^H are defined as

$$\begin{aligned} D_z^F = {} & \frac{2}{3}\left(\frac{d}{h_c}\right)^3 \cos^2\theta + \frac{2}{3}\frac{I_c}{I_f}\left[\frac{1}{8}\left(\frac{p}{h_c}\right)^3 - \left(\frac{b}{h_c}\right)^3\right] \\ & + \frac{R}{h_c}\left[2\left(\frac{b}{h_c}\right)^2\theta - 4\frac{Rb}{h_c^2}(1-\cos\theta) + \left(\frac{R}{h_c}\right)^2(\theta - \sin\theta\cos\theta)\right] \\ & + \frac{I_c}{h_c^2 t_c}\left[2\frac{d}{h_c}\sin^2\theta + \frac{R}{h_c}(\theta - \sin\theta\cos\theta)\right] \end{aligned} \tag{A-12}$$

$$\begin{aligned} D_y^H = {} & \frac{2}{3}\left(\frac{d}{h_c}\right)^3 \sin^2\theta + \frac{1}{2}\left(\frac{R}{h_c}\theta + \frac{1}{2}\frac{f}{h_c}\frac{I_c}{I_f}\right) \\ & - \left(\frac{R}{h_c}\right)^2\left[\left(2 - 3\frac{R}{h_c}\right)(\theta - \sin\theta) + \frac{R}{h_c}\sin\theta(1-\cos\theta)\right] \\ & + \frac{I_c}{h_c^2 t_c}\left[\frac{f}{h_c}\frac{t_c}{t_f} + 2\frac{d}{h_c}\cos^2\theta + \frac{R}{h_c}(\theta + \sin\theta\cos\theta)\right] \end{aligned} \tag{A-13}$$

$$\begin{aligned} D_z^H = {} & \frac{2}{3}\left(\frac{d}{h_c}\right)^3 \sin\theta\cos\theta + \frac{1}{2}\frac{I_c}{I_f}\left[\frac{1}{4}\left(\frac{p}{h_c}\right)^2 - \left(\frac{b}{h_c}\right)^2\right] \\ & + \frac{R}{h_c}\left\{\frac{b}{h_c}\theta - 2\frac{Rb}{h_c^2}(\theta - \sin\theta) - \frac{R}{h_c}(1-\cos\theta)\left[1 - \frac{R}{h_c}(1-\cos\theta)\right]\right\} \\ & - \frac{I_c}{h_c^2 t_c}\left(2\frac{d}{h_c}\sin\theta\cos\theta + \frac{R}{h_c}\sin^2\theta\right) \end{aligned} \tag{A-14}$$

where $b(=\frac{1}{2}(p-f))$ is one half of the horizontal projected length of the nonhorizontal region of the corrugation leg (fig. 5), and the moments of inertia I_f and I_c of the flat and diagonal regions of the corrugation leg are defined respectively as

$$I_f = \frac{1}{12}t_f^3 \quad , \quad I_c = \frac{1}{12}t_c^3 \tag{A-15}$$

In case 2 core orientation, subscripts x and y in equations (A-1) through (A-5) are interchanged.

Honeycomb-core sandwich, case 1 core orientation

$$D_x = E_x I_s \tag{A-16}$$

$$D_y = E_y I_s \tag{A-17}$$

$$D_{xy} = 2G_{xy}I_s \tag{A-18}$$

$$D_{Qx} = G_{cxz}h_c' \tag{A-19}$$

$$D_{Qy} = G_{cyz}h_c' \tag{A-20}$$

where h_c' is the honeycomb-core depth (fig. 2) defined as

$$h_c' = h - t_s \tag{A-21}$$

In case 2 core orientation, subscripts x and y in equations (A-16) through (A-20) are interchanged.

REFERENCES

1. Plank, P.P., I.F. Sakata, G.W. Davis, and C.C. Richie, *Hypersonic Cruise Vehicle Wing Structure Evaluation*, NASA CR-1568, 1970.

2. Greene, Bruce E., *Substantiation Data for Advanced Beaded and Tubular Structural Panels-Volume 1, Design and Analysis*, NASA CR-132460, 1974.

3. Musgrove, Max D., and Russell F. Northrop, *Substantiation Data for Advanced Beaded and Tubular Structural Panels-Volume 2, Fabrication*, NASA CR-132482, 1974.

4. Hedges, Philip C., and Bruce E. Greene, *Substantiation Data for Advanced Beaded and Tubular Structural Panels-Volume 3, Testing*, NASA CR-132515, 1974.

5. Musgrove, Max D., and Bruce E. Greene, *Advanced Beaded and Tubular Structural Panels*, NASA CR-2514, 1975.

6. Greene, Bruce E., and Russell F. Northrop, *Design and Fabrication of René 41 Advanced Structural Panels*, NASA CR-132646, 1975.

7. Musgrove, Max D., Bruce E. Greene, John L. Shideler, and Herman L. Bohon, "Advanced Beaded and Tubular Structural Panels," *J. Aircraft*, vol. 11, no. 2, Feb. 1974, pp. 68–75.

8. Shideler, John L., Herman L. Bohon, and Bruce E. Greene, "Evaluation of Bead-Stiffened Metal Panels," AIAA Paper No. 75–815, May 1975.

9. Siegel, William H., *Experimental and Finite Element Investigation of the Buckling Characteristics of a Beaded Skin Panel for a Hypersonic Aircraft*, NASA CR-144863, 1978.

10. Shideler, John L., Roger A. Fields, and Lawrence F. Reardon, *Tests of Beaded and Tubular Structural Panels, Recent Advances in Structures for Hypersonic Flight*, NASA CP-2065, Part II, 1978, pp. 539–576.

11. Ko, William L., John L. Shideler, and Roger A. Fields, *Buckling Characteristics of Hypersonic Aircraft Wing Tubular Panels*, NASA TM-87756, 1986.

12. Tenney, Darrel R., W. Barry Lisagor, and Sidney C. Dixon, "Materials and Structures for Hypersonic Vehicles," *J. Aircraft*, vol. 26, no. 11, Nov. 1989, pp. 953–970.

13. Ko, William L., "Elastic Stability of Superplastically Formed/Diffusion-Bonded Orthogonally Corrugated Core Sandwich Plates, " AIAA Paper No. 80–0683, May 1980.

14. Ko, William L., *Comparison of Structural Behavior of Superplastically Formed/Diffusion-Bonded Sandwich Structures and Honeycomb Core Sandwich Structures*, NASA TM-81348, 1980.

15. Libove, Charles, and S.B. Batdorf, *A General Small-Deflection Theory for Flat Sandwich Plates*, NACA TN-1526, 1948.

16. Bert, Charles W., and K.N. Cho, "Uniaxial Compressive and Shear Buckling in Orthotropic Sandwich Plates by Improved Theory," AIAA Paper No. 86–0977, May 1986.

17. Batdorf, S.B., and Manuel Stein, *Critical Combinations of Shear and Direct Stress for Simply Supported Rectangular Flat Plates*, NACA TN-1223, 1947.

18. Stein, Manuel, and John Neff, *Buckling Stresses of Simply Supported Rectangular Flat Plates in Shear*, NACA TN-1222, 1947.

19. Libove, Charles, and Ralph E. Hubka, *Elastic Constants for Corrugated-Core Sandwich Plates*, NACA TN-2289, 1951.

NASA
National Aeronautics and
Space Administration

Report Documentation Page

1. Report No. NASA TM-4290	2. Government Accession No.	3. Recipient's Catalog No.
4. Title and Subtitle Combined Compressive and Shear Buckling Analysis of Hypersonic Aircraft Structural Sandwich Panels		5. Report Date May 1991
		6. Performing Organization Code
7. Author(s) William L. Ko and Raymond H. Jackson		8. Performing Organization Report No. H-1694
		10. Work Unit No. RTOP 532-09-01
9. Performing Organization Name and Address NASA Dryden Flight Research Facility P.O. Box 273 Edwards, California 93523-0273		11. Contract or Grant No.
		13. Type of Report and Period Covered Technical Memorandum
12. Sponsoring Agency Name and Address National Aeronautics and Space Administration Washington, DC 20546-3191		14. Sponsoring Agency Code

15. Supplementary Notes

16. Abstract

The combined-load (compression and shear) buckling equations were established for orthotropic sandwich panels by using the Rayleigh-Ritz method to minimize the panel total potential energy. The resulting combined-load buckling equations were used to generate buckling interaction curves for super-plastically-formed/diffusion-bonded titanium truss-core sandwich panels and titanium honeycomb-core sandwich panels having the same specific weight. The relative combined-load buckling strengths of these two types of sandwich panels are compared with consideration of their sandwich core orientations. For square and nearly square panels of both types, the combined load always induces symmetric buckling. As the panel aspect ratios increase, antisymmetric buckling will show up when the loading is shear-dominated combined loading. The square panel (either type) has the highest combined buckling strength, but the combined load buckling strength drops sharply as the panel aspect ratio increases. For square panels, the truss-core sandwich panel has higher compression-dominated combined-load buckling strength. However, for shear dominated loading, the square honeycomb-core sandwich panel has higher shear-dominated combined load buckling strength.

17. Key Words (Suggested by Author(s)) Combined load buckling Honeycomb cores Sandwich panels Truss cores		18. Distribution Statement Unclassified — Unlimited Subject category 39	
19. Security Classif. (of this report) Unclassified	20. Security Classif. (of this page) Unclassified	21. No. of Pages 36	22. Price A03

NASA FORM 1626 OCT 86

For sale by the National Technical Information Service, Springfield, Virginia 22161-2171

NASA-Langley, 1991